

Best practices recommendations for estimating dissipation rates from shear probes

Rolf Lueck^{1,*}, Ilker Fer², Cynthia Bluteau³, Marcus Dengler⁴, Peter Holtermann⁵, Ryuichiro Inoue⁶, Arnaud LeBoyer⁷, Sarah-Anne Nicholson⁸, Kirstin Schulz⁹, Craig Stevens^{10,11}

¹ Rockland Scientific, Inc., Victoria, British Columbia, Canada

² Geophysical Institute, University of Bergen, Bergen, Norway

³ Institute of Ocean Sciences, Fisheries and Oceans Canada, Sidney British Columbia, Canada

⁴ GEOMAR Helmholtz Centre for Ocean Research Kiel, Kiel, Germany

⁵ Leibniz Institute for Baltic Sea Research, Warnemünde, Rostock, Germany

⁶ Japan Agency for Marine-Earth Science and Technology, Yokosuka, Kanagawa, Japan

⁷ Scripps Institution of Oceanography, UC San Diego, United States

⁸ Southern Ocean Carbon-Climate Observatory, Council for Scientific and Industrial Research, Cape Town, South Africa

⁹ Oden Institute for Computational Engineering and Sciences, The University of Texas at Austin, Austin, TX, United States

¹⁰ National Institute for Water and Atmospheric Research, Wellington, New Zealand

¹¹ Dept. Physics, University of Auckland, Auckland, New Zealand

Correspondence*:

Rolf Lueck, Rockland Scientific, Inc., 520 Dupplin Rd., Victoria, British Columbia, V8Z 1C1, Canada

rolf@rocklandsscientific.com

2 ABSTRACT

As a part of the Scientific Committee on Oceanographic Research (SCOR) Working Group #160 "Analysing ocean turbulence observations to quantify mixing" (ATOMIX), we have developed recommendations on best practices for estimating the rate of dissipation of kinetic energy, ε , from measurements of turbulence shear using shear probes. The recommendations provided here are platform-independent to the extent possible and cover the conceivable range of dissipation rates in the ocean, seas, and other natural waters. They are applicable to commonly deployed platforms that include vertical profilers, fixed and moored instruments, self-propelled ocean gliders, and other autonomous underwater vehicles. The procedure for preparing the shear data for spectral estimation is discussed in detail, as are the quality control metrics that should accompany each estimate of ε . The methods are illustrated using a high-quality 'benchmark' dataset, while potential pitfalls are demonstrated with a second dataset containing common faults.

Keywords: Turbulence, rate of dissipation, kinetic energy, shear variance

1 INTRODUCTION

15 Turbulent mixing in the ocean is an important process that influences the modification of water masses,
16 large-scale ocean currents, and the redistribution of heat, nutrients, and carbon (Wunsch and Ferrari, 2004;
17 Gregg, 2021). Thus, understanding and accurately representing turbulent mixing is essential for describing
18 ocean stratification and circulation, modeling the ocean, and predicting climate change. The viscous rate
19 of dissipation of turbulence kinetic energy, ε , is a key parameter that quantifies turbulent mixing, but its
20 observation has been notoriously difficult, making it one of the least observed of the important variables
21 for ocean climate science (Waterhouse et al., 2014). In recent years, there have been significant advances
22 and diversification in technologies (e.g., autonomous platforms, Fer et al., 2014; Nagai et al., 2015;
23 Frajka-Williams et al., 2022) available to measure and estimate ε , and consequently, a proliferation in
24 the observations of oceanic turbulence and in the number of researchers collecting such data. However,
25 there are currently no standards for processing and archiving derived turbulence estimates from these
26 observations.

27 Before the turn of the century, the measurement of oceanic turbulence was conducted by a small number of
28 research groups who each developed their own methods of calculating ε . These research groups have made
29 some intercomparisons, but the statistical nature of ocean turbulence requires many repeated measurements
30 to make these difficult comparisons (Moum et al., 1995). Because the research groups were experts on
31 ocean turbulence, the comparisons were generally good. More recently, the number of researchers using
32 shear probes has increased dramatically, while their level of expertise now has a far more extensive range
33 than previously. Some researchers would not consider themselves experts – for them, ε provides the
34 background for the study of biological and chemical processes to determine the vertical fluxes of heat,
35 nutrients, and dissolved oxygen. Consequently, they are less able to identify issues with their ε estimates.

36 Because of the recent proliferation of shear-probe users, there is a pressing need to develop best practices
37 for dissipation estimates. Such a "standard" method may contain some flaws. However, this groundwork is
38 still helpful because the best practices can be quickly and universally rectified when improvements are
39 made as new work identifies potential issues.

40 In 2020, the Scientific Committee on Oceanographic Research (SCOR) approved a Working Group on
41 "Analysing ocean turbulence observations to quantify mixing" (ATOMIX). The group's primary goal was
42 to consolidate knowledge and methods of estimating ε from turbulence measurements while developing
43 best practices and quality-control metrics for determining ε . Another objective is to establish an open-
44 access database of benchmark datasets that can be used to assess and validate algorithms for estimating
45 ε irrespective of programming language. More details can be found in the wiki site of ATOMIX, where
46 some content of this paper is summarized together with related nomenclature, required and recommended
47 parameters and metadata, and dataset formats for publication and archiving (https://wiki.app.uib.no/atomix/index.php/Main_Page). Three subgroups deal with the specifics of shear probes,
48 acoustic Doppler current profilers, and point-velocity measurements. This paper concentrates on ATOMIX's
49 subgroup about ε estimates made from shear-probe data. A focus of the shear-probe group of ATOMIX
50 has been to envelop estimates of dissipation rates and shear spectra with statistical uncertainty estimates.
51 The statistical reliability of an estimate of a spectrum of shear and an estimate of the dissipation rate have
52 been explored by Lueck (2022b) and Lueck (2022a). Our recommendations are platform-independent to
53 the extent possible, meaning that the described procedure can be applied to any device that samples the
54 required set of parameters. They are hence applicable to commonly deployed platforms that include vertical
55 profilers, fixed and moored instruments, self-propelled ocean gliders, and other autonomous underwater
56 vehicles.
57

58 In section 2, we provide background information about the technology and theoretical framework for
59 estimating ε from shear-probe data streams. Section 3 describes the data processing steps for obtaining ε ,
60 descriptions of the confidence intervals for spectral estimates and for dissipation estimates, followed by a
61 discussion about quality-control metrics. The structure of Section 3 is organized in the same fashion as the
62 recommended structure of data in ATOMIX format, such as the benchmark dataset presented in section 4,
63 and can be used to assess algorithms irrespective of the programming language used.

2 BACKGROUND

64 2.1 Shear Probes

65 The shear probe is an airfoil of revolution that was originally developed by Siddon and Ribner (1965)
 66 and Siddon (1965) for atmospheric and wind-tunnel measurements of turbulent cross-stream velocity
 67 fluctuations. The probe was subsequently modified for use in water (Siddon, 1971) and it was first deployed
 68 in 1972 on a vertical microstructure profiler in a fjord on the west coast of Canada (Osborn, 1974). Osborn
 69 and Crawford (1980) describe its theory of operation and one method of calibration. The sensing element
 70 is a two-layer piezo-ceramic beam that generates an electric charge in response to bending forces (Fig. 1).
 71 About one-half of the beam is solidly anchored into its supporting stainless steel sting, and the other half
 72 is cantilevered out of the sting and will generate a charge if it is bent. The bending under a load is in the
 73 direction normal to the wide surface of the beam – much like a diving board at the side of a swimming pool
 74 bends in the vertical direction but not in the horizontal direction. A water-blocking layer is placed over the
 75 surface of the ceramic, and the entire tip is covered with silicon rubber to form a surface of revolution –
 76 much like the shape of a bullet. A piezo-ceramic is inherently an AC-sensor. It responds only to fluctuations
 77 and produces no mean signal. The resistance of the beam must exceed $\sim 10^{10} \Omega$ in order for the shear probe
 78 to respond properly at the lowest apparent frequencies of the microstructure (~ 0.1 Hz). There are several
 79 versions of the shear probe. They differ mainly in the length of the tip measured relative to the point of the
 80 cantilever and the diameter at the point of cantilever.

81 Although the shear probe was initially used on vertical profilers, it can be used to measure the cross-
 82 profile fluctuation of velocity along any direction of profiling. Because there are always two cross-profile
 83 directions, profilers often carry two shear probes, with one rotated around its longitudinal axis by 90° ,
 84 to measure both components of shear. Shear probes have been deployed on both downward and upward
 85 vertical profilers, on gliders that profile $\approx 30^\circ$ with respect to horizontal (Fer et al., 2014; St. Laurent, 2017),
 86 on towed and self-propelled vehicles (Fleury and Lueck, 1992; Osborn et al., 1992; Naveira Garabato et al.,
 87 2019), and on moored and fixed platforms where "profiling" is provided by the ambient current (Fer and
 88 Bakhoday Paskyabi, 2014; McMillan et al., 2016).

89 2.2 The signal produced by a shear probe

90 The across-axial force produced on the shear probe by a flow is

$$F \propto \frac{1}{2} \rho U^2 \sin 2\alpha = \rho(U \cos \alpha)(U \sin \alpha) = \rho W u , \quad (1)$$

91 where U is the total incident velocity (Fig. 1), α is the angle of attack, ρ is the fluid density, and u is the
 92 cross-axial component of the flow (Allen and Perkins, 1951). The charge produced by the piezo-ceramic
 93 element is proportional to this lift force and, therefore, proportional to the cross-axis velocity u as well
 94 as to the along-axis velocity, W , i.e., the speed of profiling of the shear probe. Here we used an example
 95 of a vertical profiling instrument, hence adopting the notation W for the speed of profiling. The charge
 96 produced by the shear probe is converted into a voltage, E , by its supporting electronics and, thus,

$$E = S \rho W u , \quad (2)$$

97 where the sensitivity S accounts for the efficiency of converting mechanical energy into electrical energy
 98 by the piezo-ceramic and the charge-to-voltage conversion factor of the electronics.

99 A shear probe is typically calibrated by exposing it to a jet of water with a velocity U and a time-varying
 100 angle of attack, α (Fig. 1). The probe is spun around its longitudinal axis to generate an angle of attack that
 101 varies sinusoidally with an amplitude α (Osborn and Crawford, 1980). The sensitivity of the shear probe is
 102 determined by regressing the root-mean-square voltage E_{rms} against $U^2 \sin 2\alpha$ so that

$$E_{\text{rms}} = SU^2 \sin 2\alpha , \quad (3)$$

103 where the sensitivity, S , is the constant of proportionality. (When the shear probe was developed, it
 104 was easier to measure a root-mean-square voltage than a voltage amplitude.) The instantaneous voltage
 105 produced by the shear probe and its circuitry is then

$$E_P = \sqrt{2}SU^2 \sin 2\alpha = 2\sqrt{2} S(U \cos \alpha) (U \sin \alpha) = 2\sqrt{2} SWu , \quad (4)$$

106 where the factor of $\sqrt{2}$ comes from converting an rms voltage into a peak voltage. A typical value for S is
 107 $0.1 \text{ V m}^{-2} \text{ s}^2$.

108 2.3 Theories to estimate dissipation from shear spectra

109 Estimates of the rate of viscous dissipation of turbulence kinetic energy, ε , require the measurement
 110 of the shear signal in units of s^{-1} and the flow past the sensor, here referred to as the speed of profiling,
 111 W . The latter is needed to convert the time domain into the space domain, and frequency spectra into
 112 wavenumber spectra assuming frozen turbulence, as will be described in the procedures (Sec. 3.3). We then
 113 make use of turbulence model spectra (see below) to extract ε from these spectral observations, rather than
 114 directly from measurements in the time domain. The area under the shear spectrum is proportional to ε .

115 A typical shear spectrum (Fig. 2) rises with wavenumber, k , in proportion to $k^{1/3}$ in the inertial subrange
 116 (isr), and then diminishes rapidly with increasing k due to viscosity in the viscous subrange (vsr). Spectral
 117 models of shear are usually provided in a non-dimensional form, $\tilde{\Psi}(\tilde{k})$ and can be dimensionalized by
 118 using

$$\begin{aligned} \Psi(k) &= \left(\frac{\varepsilon^3}{\nu} \right)^{1/4} \tilde{\Psi}(\tilde{k}) , \\ k &= \tilde{k} L_K^{-1} , \\ L_K &= (\nu^3 / \varepsilon)^{1/4} , \end{aligned} \quad (5)$$

119 where ν is the temperature-dependent molecular kinematic viscosity in units of $\text{m}^2 \text{ s}^{-1}$, ε is in units of
 120 W kg^{-1} (or $\text{m}^2 \text{ s}^{-3}$), and k in units of cpm, which is non-dimensionalized using the Kolmogorov length
 121 L_K (Fig. 3). Note that the cyclic wavenumber k is different from the angular wavenumber in units of
 122 rad m^{-1} , equal to $2\pi k$. This means that the peak of the dimensional spectrum rises in proportion to $\varepsilon^{3/4}$
 123 and shifts to a higher wavenumber in proportion to $\varepsilon^{1/4}$, which is required to make the area under the
 124 spectrum proportional to ε . High dissipation rates require more bandwidth than low rates. About 25 % of
 125 the shear variance resides at wavenumbers smaller than the peak, and 95 % of the shear variance resides at
 126 wavenumbers smaller than where the spectrum has dropped by a factor of 10 below its peak (Fig. 3).

127 There are several models of the spectrum of shear. One is the values of the shear spectrum tabulated by
 128 Oakey (1982) that were derived from the along-profile velocity spectrum reported by Nasmyth (1970), and

129 was originally approximated by Wolk et al. (2002) using

$$\tilde{\Psi}_{N_1}(\tilde{k}) = \frac{8.05 \tilde{k}^{1/3}}{1 + (20.6 \tilde{k})^{3.715}}, \quad (6)$$

130 who deem the 8-th spectral value to be erroneous because it is above the $k^{1/3}$ tendency of the inertial
 131 subrange (Fig. 3, red). The approximation by Lueck (2022a) of the values tabulated by Oakey (1982) that
 132 includes the 8-th spectral value is

$$\begin{aligned} \tilde{\Psi}_{N_2}(\tilde{k}) &= \frac{7.89 \tilde{k}^{1/3}}{1 + (21.2 \tilde{k})^3} \left(\frac{1}{1 + (6 \tilde{k})^{5/2}} \right) \left(1 + \frac{0.11 y}{(y-1)^2 + y/2} \right), \\ y &= \left(\frac{\tilde{k}}{0.019} \right)^2 \end{aligned} \quad (7)$$

133 (Fig. 3, black). For this approximation, the values reported by Oakey (1982) were increased by 2 % so that
 134 the integral of this spectrum equals 2/15. Lueck (2022a) also provides an approximation that is based on
 135 more than 14 000 spectra of shear collected with shear probes, which is given by

$$\begin{aligned} \tilde{\Psi}_L(\tilde{k}) &= \frac{8.048 \tilde{k}^{1/3}}{1 + (21.7 \tilde{k})^3} \left(\frac{1}{1 + (6.6 \tilde{k})^{5/2}} \right) \left(1 + \frac{0.36 y}{(y-1)^2 + 2y} \right), \\ y &= \left(\frac{\tilde{k}}{0.015} \right)^2 \end{aligned} \quad (8)$$

136 (Fig 3, maroon). Panchev and Kesich (1969) developed a three-dimensional velocity spectrum and Roget
 137 et al. (2006) used it to provide an approximation of shear spectrum that reads

$$\tilde{\Psi}_{PK}(\tilde{k}) = 11.9 \tilde{k}^{0.372} \exp(-90.9 \tilde{k}^{1.495}) \quad (9)$$

138 (Fig 3, green). Note that $\tilde{\Psi}_{PK}$ rises more steeply than $k^{1/3}$ at low wavenumbers. These approximations
 139 differ by $\sim 15\%$, any of them can be used as a reference for comparison against a measured spectrum and
 140 the integrals of these approximations (Eq. 11) can be used to estimate the variance of shear that may be
 141 missing because of spectral integration to a finite wavenumber.

142 For typical oceanographic turbulence levels, $\varepsilon \lesssim 10^{-5} \text{ W kg}^{-1}$, shear probes can resolve a sufficient
 143 fraction of the shear variance in the viscous subrange. Using the viscous subrange and assuming isotropic
 144 turbulence, ε can be estimated from any single component of shear, using

$$\varepsilon = \frac{15}{2} \nu \overline{\left(\frac{\partial u}{\partial z} \right)^2} = \frac{15}{2} \nu \int_0^\infty \Psi(k) dk \approx \frac{15}{2} \nu \int_{k_l}^{k_u} \Psi(k) dk \quad (10)$$

(Taylor, 1935). The small-scale isotropy describes a state whereby the velocity components at dissipation scales and their derivatives are independent of direction, i.e., they do not have a preferred orientation and appear similar from all points of view. The largest scale eddies of a turbulent flow contain the bulk of the turbulence kinetic energy of the flow. The isotropic equation (10) is valid for the variance of any shear component, i.e., the most relevant formulation for shear probes. When one of the axial derivatives, i.e., the strain e.g., $\partial u / \partial x$, is preferred for a different type of sensor, the factor 15/2 must be replaced by 15.

The approximation in Eq. (10) gives the shear variance by integrating the wavenumber spectrum between the lower limit of spectral integration (usually $k_l = 0$, or the lowest non-zero wavenumber), and the upper limit k_u (see Sec. 3.4.1). The right-most form of Eq. (10), by limiting the bandwidth of the estimate, allows for the exclusion of noise due to the electronics, vibrations, and other sources of contamination of the measurement of shear (see the high wavenumber end of Fig. 2). Limiting the bandwidth of the estimate of ε may also exclude real shear variance and, therefore, an empirical model of turbulence shear is used to estimate the fraction of the variance that may be excluded. The approximations of the integral of the shear spectra of Eq.(6) to Eq.(9) are

$$\begin{aligned} I_{N_1}(\tilde{k}) &= \frac{15}{2} \int_0^{\tilde{k}} \tilde{\Psi}_{N_1}(\xi) d\xi = \tanh\left(48.0 \tilde{k}^{4/3}\right) - 2.9 \tilde{k}^{4/3} \exp\left(-22.3 \tilde{k}^{4/3}\right), \\ I_{N_2}(\tilde{k}) &= \frac{15}{2} \int_0^{\tilde{k}} \tilde{\Psi}_{N_2}(\xi) d\xi = \tanh\left(61.5 \tilde{k}^{4/3}\right) - 8.1 \tilde{k}^{4/3} \exp\left(-52.5 \tilde{k}^{4/3}\right), \\ I_L(\tilde{k}) &= \frac{15}{2} \int_0^{\tilde{k}} \tilde{\Psi}_L(\xi) d\xi = \tanh\left(65.5 \tilde{k}^{4/3}\right) - 9.0 \tilde{k}^{4/3} \exp\left(-54.5 \tilde{k}^{4/3}\right), \\ I_{PK}(\tilde{k}) &= \frac{15}{2} \int_0^{\tilde{k}} \tilde{\Psi}_{PK}(\xi) d\xi = \tanh\left(103 \tilde{k}^b\right) - 67 \tilde{k}^b \exp\left(-94 \tilde{k}^b\right), \end{aligned} \quad (11)$$

where $b = 1.372$ (Fig. 3, dash-dot colored lines).

In highly energetic environments ($\varepsilon \gtrsim 10^{-5} \text{ W kg}^{-1}$), such as in tidal channel flows, the upper ocean during storms, or vigorously turbulent overflows, the shear probe cannot sufficiently resolve the viscous subrange of the shear spectrum. It is thus recommended to fit the larger scales of the shear spectrum within the inertial subrange using a model spectrum. We recommend the following model of the shear spectrum in the inertial subrange:

$$\Psi_{\text{isr}}(k) = (2\pi)^{4/3} \frac{4}{3} C_1 \varepsilon^{2/3} k^{1/3} = A \varepsilon^{2/3} k^{1/3}, [\text{s}^{-2} \text{ cpm}^{-1}] \quad (12)$$

where the coefficient C_1 is the one-dimensional Kolmogorov constant for velocity fluctuations in the along-profile direction (the strain component) and has an average value of $C_1 = 0.53$ with a standard deviation of 0.055 (Sreenivasan, 1995a). The Kolmogorov constant for the shear component is $\frac{4}{3}C_1$ (Pope, 2009) and the factor of $(2\pi)^{4/3}$ is required when working in units of cpm rather than rad m^{-1} . The recommendation of Sreenivasan (1995b) gives a value of $A = 8.19$, while the models and approximations of Eq. 6 and Eq. 8 give $A = 8.05$ and Eq. 7 gives $A = 7.89$. These values span a range of $\pm 2\%$ and, therefore, all are suitable for estimating dissipation rates. The model of Panchev and Kesich (1969) is not recommended because it does not rise as $k^{1/3}$ in the inertial subrange, which is inconsistent with the velocity spectrum proposed by Kolmogorov (1941).

3 RECOMMENDED DISSIPATION ESTIMATE PROCEDURE

174 The method described here is platform independent – it can be applied to a shear probe that is mounted on
 175 any vehicle such as a vertical profiler, a glider, a self-propelled vehicle, and on a moored or fixed structure.

176 The procedure of dissipation estimation is summarized in the flow chart Fig. 4. The recommended
 177 procedure is presented in terms of levels, ranging from Level 1 to Level 4, where Level 1 is the data
 178 converted into physical units of shear, Level 2 is the selection, cleaning, and preparation of the shear data,
 179 Level 3 is its spectral estimation, and Level 4 is the estimation of the rate of dissipation, ε , from the spectra
 180 of shear and the quality control metrics that should accompany the estimates. The following subsections
 181 detail the recommendations for each step.

182 3.1 Level 1: Obtain shear data in physical units

183 Data collected with a shear probe is always in the form of integers (whole numbers), produced by a
 184 sampler, that spans a range of values related to the voltage produced by the continuous-domain electronics
 185 that support the probe. The speed past the sensor, i.e., instrument carrying platform speed with respect
 186 to water, W , is used for every sample to perform the charge-to-voltage conversion (Eq. 2). We refer to
 187 W as the speed of profiling, following the tradition of vertically profiling instruments. The speed may
 188 be available from one or more signals recorded by the instrument, or it may have to be determined from
 189 simultaneous measurements from another instrument. For example, when analyzing data collected from
 190 gliders, the flow past the shear probe and the angle of attack can be obtained from a hydrodynamic flight
 191 model of the glider, while for a vertical profiler, the rate of change of pressure may be used to deduce the
 192 speed of profiling. We emphasize that the rate of change of pressure only approximates the speed past
 193 the sensor when the profiling speed is substantially larger than the background vertical velocity. This is
 194 typically valid for profilers ballasted for target speeds greater than $\sim 0.3 \text{ m s}^{-1}$, and can be violated in more
 195 energetic eddies, or in the presence of strong wave orbital velocities near the ocean surface.

196 The cross-profile velocity signal produced by the shear probe (Eq. 4) must be converted into a shear
 197 signal. In some instruments, this is done in analogue before the continuous-domain shear-probe signal is
 198 sampled, by passing it through a time-differentiator circuit to produce a varying voltage

$$E_{dt} = \gamma G_D \frac{d}{dt} E_P = 2\sqrt{2} \gamma S W G_D \frac{du}{dt}, \quad (13)$$

199 where G_D is the gain of the differentiator in units of s , and γ is the number-to-voltage conversion rate
 200 of the sampler. It is this continuous-domain signal that is usually sampled and recorded. Finally, the
 201 discrete-domain signal of shear is derived using

$$\frac{\partial u}{\partial z} = \frac{1}{W} \frac{du}{dt} = \frac{E_{dt}}{2\sqrt{2} \gamma G_D S W^2}. \quad (14)$$

202 The manufacturer of the electronics must provide the value of the differentiator gain, G_D , the sensitivity, S ,
 203 and the conversion rate of the sampler, γ . An estimate of the speed of profiling, W , is then used to complete
 204 the conversion of the dimensionless samples into a shear signal with physical units of s^{-1} . Note that the
 205 shear is sensitive to the speed of profiling, $\propto W^{-2}$, and the shear variance, hence ε through Eq. (10),
 206 $\propto W^{-4}$.

207 For an instrument that does not electronically differentiate the continuous-domain shear-probe signal
 208 before sampling, the shear-probe data must be converted to shear in the discrete-domain. This is achieved

209 by one of two means. The first method involves taking the Fourier transform of the velocity samples,
 210 multiplying this transform by $2\pi j f$ where f is the frequency of the transformed samples, $j^2 = -1$, and
 211 converting the multiplied transform back into the time domain using the inverse Fourier transform. This
 212 provides the rate of change of the velocity signal and is similar (but not exactly equal) to that obtained by a
 213 continuous-domain differentiator. This signal can be converted into a shear signal by dividing it by the
 214 profiling speed. The second method of obtaining the rate-of-change of the sampled velocity signal involves
 215 using a first-difference operation, such as,

$$\frac{du(n)}{dt} = f_s [u(n) - u(n - 1)] \quad (15)$$

216 where f_s is the sampling rate. This is, however, only an approximation of a derivative that is asymptotically
 217 correct only in the limit of zero frequency and underestimates the derivative at higher frequencies. Spectra
 218 of shear derived from this approximation have to be recolored by multiplying them by the factor

$$\left(\frac{\pi}{2} \frac{f}{f_N}\right)^2 \left[\sin\left(\frac{\pi}{2} \frac{f}{f_N}\right)\right]^{-2} \quad (16)$$

219 where $f_N = \frac{1}{2}f_s$ is the Nyquist frequency to account for the difference between the approximation of
 220 Eq.(15) and a continuous-domain time derivative (Antoniou, 1979). This correction factor rises from unity
 221 at zero frequency to $\pi^2/4 \approx 2.47$ at the Nyquist frequency. In the method of processing discussed below,
 222 we assume that the samples represent a true time derivative and leave it to a user to make the spectral
 223 correction if they use a first-difference approximation to create a time derivative.

224 In addition, it may be necessary to make other spectral corrections if the manufacturer of the instrument
 225 modifies the frequency content of measurements in the band of interest for dissipation estimation.

226 3.2 Level 2: Prepare time series sections for analysis**227 3.2.1 Section selection**

228 We must select the ranges within our data file (sections) that are suitable for analysis. A section is a
229 continuous part of a time series that has been selected for dissipation estimates. For example, if the data
230 come from an ascending profiler, only the data collected on the upcast are good for turbulence analysis. If
231 the data were collected continuously while this instrument descended and ascended successively five times,
232 the file could contain five data sections that correspond to the upward profiles. If an instrument mounted
233 on a glider collected data continuously, the data recorded between the turning points at which the glider
234 behavior changes from a descent to an ascent, would form separate sections. If the measurement platform
235 speed with respect to water (generally referred to as the "profiling speed") reduces to levels at which shear
236 probes cannot reliably operate, new sections must be selected. This can happen, for example, when a glider
237 stalls in response to strong currents or near the turning points, during periods of weak currents or reversals
238 in a moored system, and when the free-fall or free-rise of a vertically profiling instrument is interrupted by
239 an operator or by strong updrafts in the water column. Thus, the shear time series in Level L1 can contain
240 as little as a single section that lasts for only a few seconds, to as much as multiple sections that last for
241 hours.

242 A measurement platform must satisfy certain threshold criteria for the measurements of shear to be
243 valid for the estimation of the rate of dissipation. These criteria include a minimum speed of profiling,
244 a maximum pitching and rolling, a maximum acceleration, and a minimum depth. These criteria must
245 be satisfied for some minimum duration so that the section can produce at least one estimate of the rate
246 of dissipation, ε . The response of the shear probe is fairly linear for angles of attack smaller than $\sim 20^\circ$.
247 Pitching and rolling motions beyond this level will likely lead to non-linearity and other spurious effects
248 and should be excluded from further analysis. When a vertical profiler is suspended near the surface over
249 the vessel's side, it will have a vertical velocity that oscillates around zero. Data collected at this time fails
250 the speed and pitching criteria and so are unsuitable for analysis. After an instrument is released, it will
251 accelerate and reach $\approx 90\%$ of its terminal fall rate in about one body length – a characteristic that may be
252 slightly instrument dependent. Data collected during this period should also be excluded from analysis
253 as it will fail the speed and acceleration criteria. Data collected during acceleration can be excluded by
254 setting a minimum speed (80 to 90 % of the known fall rate of an instrument) and a minimum depth that
255 is more than two times the length of the profiler. Another suitable minimum depth must be deeper than
256 the vessel's draft used to deploy a profiler. This is because the vessel hull will likely be disturbing the
257 water column. In quiescent conditions or using larger vessels, this minimum depth may be $1.5 \times$ the ship's
258 draft. If the measurement platform slows down below the minimum speed of the profiling threshold during
259 data collection, a new section begins when the instrument reaches its terminal speed again for a minimum
260 required duration. These conditions must be satisfied for a duration that equals the length of data we plan to
261 use for each dissipation estimate divided by the speed of the profiler. The length of data record that should
262 be used for an estimate of ε depends on a number of factors, including statistical uncertainty of an estimate
263 (Sec. 3.3.5), and is often determined interactively.

264 3.2.2 Cleaning shear-probe data

265 Collisions of the shear probe with plankton and other matter do occur and can greatly bias the variance of
266 shear reported by a probe. Such encounters usually result in "data spike" - a rapid rise (or fall), followed by
267 a reversal, and a ringing with decaying amplitude, for a duration of ≈ 50 ms (Fig. 5). Collisions with larger
268 entities such as jellyfish and seaweed cause longer-lasting anomalies. Anomalous shear due to collisions

must be removed from the shear-probe signals before spectral estimation. While different methodologies for de-spiking shear-probe signals are possible, we recommend the following algorithm to remove spikes effectively, using data from the whole L1 section (i.e., after removing unused data).

- Data are high-pass filtered, forwards and backwards, with a first-order Butterworth filter with a cutoff frequency of ≈ 0.1 Hz to remove offsets and very low-frequency signals without shifting the data in time.
- The data are rectified by taking their absolute value.
- A copy of the rectified data is smoothed by filtering it forwards and backwards, with a first-order low-pass filter with a cutoff frequency that is usually in the range of 0.25 to 2 Hz.
- Samples for which the absolute to the smoothed absolute shear ratio exceeds a threshold (typically 8), are identified as spikes.
- A number, N , of samples after a spike and $N/2$ before a spike are replaced by a constant value equal to the mean shear of an approximately one-half second interval before and after the range of replacement.

These steps are repeated until there are no samples that exceed the threshold. The recommended algorithm and the choice of threshold values are based on experience. The purpose of the low-pass filter is to establish the typical magnitude of shear in a neighborhood that has a duration of approximately the inverse of its low-pass filter cutoff frequency. Forwards and backwards filtering imparts zero phase and no time-shift to the data. A shear sample is anomalous if its magnitude exceeds the typical magnitude by more than a factor of the threshold. Thus, if the variance of shear is small, a small anomaly is detected, while the same anomaly remains undetected if the variance of shear is large. That is, only anomalies that have the potential to bias the variance are removed. It is important to use a first-order filter because it does not cause over- and under-shoots, nor ringing, that could generate negative signals.

What is a suitable neighborhood and low-pass cutoff frequency? Turbulent patches in the ocean are seldom thinner than about 0.5 m in the vertical direction. This can serve as a lower limit to the definition of a neighborhood and an upper limit to the cutoff frequency. Thus, if a vertical profiler is moving at a speed of W , then the low-pass cutoff frequency should be no larger than $\approx 0.5/W$. Gliders that profile at an angle of $\approx 30^\circ$ should use a cutoff frequency based on their vertical velocity rather than their profiling speed.

The response of the probe to a collision is a temporal one. A certain duration of shear data should be modified to remove the anomaly. Typically, the data are replaced 20 ms (i.e. around 10 samples for a sampling rate of 512 Hz) before a spike for the initial run-up to the first extrema and 40 ms (i.e. around 20 samples) after the last extrema for the decaying oscillation. The de-spiking should be applied iteratively to remove anomalies that last longer than 60 ms. The fraction of the data altered by a de-spiking routine must be noted for each data segment used to estimate a spectrum of shear because this quality-control metric should not exceed a few percent. There is currently no standard for what is an acceptable fraction of modified (de-spiked) data. The number of passes or attempts made to clean the shear-probe data is a quality-control metric. If many attempts are required to clean the data then the anomalies are extremely long and may be caused by collisions with objects larger than the typical size of zooplankton such as, for example, jellyfish. While there is no objective criterion for the maximum number of passes that should be tolerated, experience indicates that data requiring more than 8 passes are very unusual and should not be used for the estimation of the rate of dissipation.

310 3.2.3 High-pass filter time series

311 Although the shear probe inherently senses only zero-mean fluctuations, its electronics may impart a
 312 non-zero mean that should be removed by digital high-pass filtering. Once the data have been cleaned by
 313 removing shear anomalies, it can be filtered. The cutoff frequency for digital high-pass filtering must be
 314 decided at this stage. The recommended high-pass filter is a first-order Butterworth filter with a cutoff
 315 frequency of approximately one-half of the lowest frequency resolved by the spectra for dissipation
 316 estimates. The lowest frequency resolved is the inverse of the FFT length (in s), namely $f_l = \tau_{\text{fft}}^{-1}$. Thus,
 317 the recommended choice for high-pass filtering of the shear data is

$$f_{\text{HP}} = \tau_{\text{fft}}^{-1}/2 . \quad (17)$$

318 The choice of other spectral parameters is described in the next section.

319 3.3 Level 3: Produce wavenumber spectra of shear and related sensors

320 The shear variance is obtained from a wavenumber spectrum of shear time series that is cleaned (de-
 321 spiked) and high-pass filtered as described earlier. Here we describe (i) how the wavenumber spectrum
 322 should be calculated, (ii) its correction for the high-pass filter, and (iii) the removal of vibration-coherent
 323 contamination.

324 3.3.1 Spectral calculations

325 The estimation of spectra and dissipation rates requires setting a number of parameters, including the
 326 data length for each dissipation estimate and the length of the FFT segments (FFT length). This choice
 327 of parameters should be governed by the scientific objectives for the dissipation estimate. The lowest
 328 wavenumber of the spectrum is the lowest resolved frequency divided by the speed of profiling, $k_l = f_l/W$.
 329 Spectra for dissipation rates that are low ($\varepsilon \lesssim 10^{-9} \text{ W kg}^{-1}$), moderate ($\varepsilon \lesssim 10^{-7} \text{ W kg}^{-1}$), and high
 330 ($\varepsilon \gtrsim 10^{-7} \text{ W kg}^{-1}$), are well resolved by k_l equal to ≈ 0.5 , ≈ 1 , and ≈ 2 cpm, respectively. For an instrument
 331 with a slow profiling speed of 0.3 m s^{-1} , FFT lengths of 7 s are needed to resolve $k_l = 0.5 \text{ cpm}$, whereas a
 332 profiling speed of 1 m s^{-1} requires FFT lengths of 2 s.

333 The FFT length, when converted to meters (i.e., an FFT length of 2 s for a 0.5 m s^{-1} profiling speed
 334 corresponds to an FFT length of 1 m), should never exceed the length of a (free) profiler because the profiler
 335 will be advected by eddies comparable to and larger than the profiler, which diminishes the large-scale
 336 shear measured by the shear probe.

337 The FFT segments should be individually detrended by either a zero-order or a first-order polynomial to
 338 minimize the zero-frequency spectral value (which is assumed to be zero) and to reduce the leakage of
 339 low-frequency content into the first non-zero frequency spectral estimate. Higher-order detrending removes
 340 low-frequency variance and is not recommended.

341 Because turbulence shear is a broad-banded signal (one with a spectrum that does not change rapidly with
 342 respect to wavenumber), the detrended FFT segments should be windowed *and* overlapped to increase the
 343 statistical reliability of the spectrum. Here, windowing means multiplying the time series record in the FFT
 344 segment by a window shape that varies smoothly from zero at the start of a segment, reaches a peak, and
 345 decreases symmetrically to zero at the end of the segment. It is important to do both. Neither windowing
 346 without overlap nor overlapping without a window increases the statistical reliability of a spectrum. The
 347 actual window used is not critical (Nuttall, 1971) but it should be scaled to have a mean-square equal to 1,
 348 so that it does not change the variance of the signal. We recommend a cosine window with 50 % overlap

349 between adjacent segments. Thus, a data length that is twice as long as the FFT length uses three FFT
 350 segments ($N_f = 3$) for the spectral estimate and should be considered the absolute minimum length.

351 The length of data to use for a spectral estimate depends on the desired spatial resolution of the ε estimates.
 352 This is a scientific question and cannot be determined here. However, the statistical reliability of a spectral
 353 estimate depends on the number of FFT segments, N_f , used to estimate the spectrum (Eq.22), and impacts
 354 the uncertainty of a dissipation estimate (Eq.29). We do not recommend using fewer than three segments
 355 unless there is a pressing need for very high spatial resolution of the ε estimates. Using the above example
 356 of an FFT length of 1 m with 50 % overlap between adjacent segments, a dissipation estimate length of
 357 4 m corresponds to $N_f = 7$. It is common to overlap the data used for the dissipation estimate by 50 %,
 358 yielding, for this example, a spatial resolution of ε of 2 m. Another point that should be considered is the
 359 assumption of stationarity over the dissipation estimate length. Particularly near the boundary layers where
 360 the dissipation rate profile can change strongly with depth, or in parts of the time series with substantial
 361 acceleration or deceleration of profiling speed, large values of N_f can violate the stationarity assumption.

362 3.3.2 Correction for the spatial response

363 The shear probe has a frequency response determined by the probe tip's mechanical stiffness and mass.
 364 Vibration tests indicate that the frequency response is several kilo-hertz and, therefore, not an issue at
 365 the usual speeds of profiling. However, its finite size does induce spatial averaging which limits the
 366 wavenumber response of the shear probe. Macoun and Lueck (2004) indicate that the response of their
 367 probes have the form of a first-order low-pass filter with a half-power wavenumber of $k_0 = 50$ cpm. That
 368 is, the measured spectrum is reduced by the factor

$$H(k) = \frac{1}{1 + (k/k_0)^2}, \quad (18)$$

369 where k is the wavenumber in units of cpm. This response was determined for a probe with a length of
 370 9.5 mm from tip to fulcrum and diameter of 5 mm at its fulcrum. The response scales with the size of
 371 the probe and may be different for other probes. Spectra of shear must be multiplied by the inverse of
 372 Eq. (18) to correct them for the spatial averaging by the shear probe. Note that this correction amplifies the
 373 spectrum by a factor of 10 at a wavenumber of 150 cpm, and it is not recommended to use the spectrum at
 374 wavenumbers where the correction exceeds a factor of 10.

375 3.3.3 Correction for high-pass filter

376 Digital filters are not perfect as they attenuate the spectra at frequencies smaller than the cutoff frequency.
 377 The spectra should be corrected for the first-order, high-pass filter applied both forwards and backwards at
 378 Level 2. The spectral correction is the inverse of the magnitude-squared response of such a filter which is

$$|H_{HP}(f)|^{-2} = \left[1 + \left(\frac{f_{HP}}{f} \right)^2 \right]^2. \quad (19)$$

379 where f_{HP} is the high-pass cut-off frequency. For the recommended high-pass cut-off frequency of Eq.(17),
 380 the correction at the lowest (non-zero) frequency of the spectrum, namely $f = \tau_{fft}^{-1}$, is only a factor of
 381 $(5/4)^2$, and this factor diminishes rapidly to unity with increasing frequency.

382 3.3.4 Vibration-coherent noise removal

383 If there are concurrent measurements of the acceleration, or the vibration, of the platform that carries the
 384 shear probes, and if they are sampled at the same rate as the shear probes, then these measurements should
 385 be used to remove those parts of the shear signals that are coherent with the vibrations. (A vibration sensor
 386 measures only the time-varying part of an acceleration.) For this removal, we recommend the method of
 387 Goodman et al. (2006), which removes from a multi-variate measured shear spectrum, $\Psi_{ij}(f)$, vibrations
 388 that are coherent with the shear-probe signals using

$$\Psi_{ij} = \hat{\Psi}_{ij} - \chi_{ik} \Gamma_{kl}^{-1} \chi_{lj}^* \quad (20)$$

389 where Ψ_{ij} and $\hat{\Psi}_{ij}$ are the corrected (de-contaminated) and original cross-spectrum of the i -th and the j -th
 390 shear-probe signals, χ_{ij} is the cross-spectrum of the shear-probe and vibration signals, Γ_{ij} is the cross-
 391 spectrum of the vibration (and possibly other) signals that are contaminating the shear-probe measurements,
 392 the superscript * indicates a complex conjugate, and summation over repeated indices is implied. All of
 393 these quantities are functions of frequency (or wavenumber).

394 The term ‘cross-spectrum’ needs some clarification. The cross-spectrum of the i -th and the j -th shear-
 395 probe signals is a three-dimensional and complex matrix that has dimensions of $P \times P \times N$ where P
 396 is the number of shear signals, and N is the number of frequency indices in the cross-spectrum. The
 397 auto-spectra of the shear signals are on the diagonal of this three-dimensional cross-spectrum. For example,
 398 $\Psi_{22}(f)$ is the auto-spectrum of the signal from shear probe 2. It is real. The off-diagonal elements are
 399 the cross-spectra between pairs of shear probes. For example, $\Psi_{12}(f) = \Psi_{21}^*(f)$ is the cross-spectrum of
 400 probes 1 and 2. It is complex. The cross-spectrum of vibrations, Γ_{ij} , has dimensions $M \times M \times N$ where
 401 M is the number of vibration signals that are used to remove coherent noise from the shear-probe signals.
 402 The cross-spectrum of the i -th shear-probe and the j -th vibration signals, χ_{ij} , has dimensions $P \times M \times N$,
 403 and is entirely complex.

404 The technique of Goodman et al. (2006) relies on estimating the (squared-) coherency between the
 405 vibration and shear-probe signals. The second term on the right hand side of Eq.(20) is the coherency
 406 times the cross-spectrum of shear. Coherency is a positive definite quantity and is always finite, even for
 407 completely unrelated signals, when the number of FFT segments used to make its estimate is finite. That is,
 408 it underestimates the corrected spectrum $\Psi_{ij}(f)$ by a factor of

$$R = 1 - 1.02 \frac{N_V}{N_f} \quad (21)$$

409 where N_V is the number of vibration (and other) signals used to remove vibration-coherent noise from the
 410 shear-probe spectra, and N_f is the number of FFT segments used to make the estimate (Ferron et al., 2023).
 411 The spectrum of shear is corrected by dividing it by R . The factor of 1.02 in Eq.(21) holds strictly for the
 412 recommended cosine window with 50 % overlap. However, it is nearly identical for other windows and for
 413 all overlaps that are smaller than $\approx 2/3$. For the example $N_f = 7$ and using two vibration sensors $N_V = 2$,
 414 we obtain $R = 0.7086$.

415 3.3.5 Uncertainty of a shear spectrum

416 The statistical reliability of an estimate of a spectrum of shear has a probability density function (pdf)
 417 that is log-normal, and has been explored by Lueck (2022a). The statistical uncertainty of an estimate of

418 the natural logarithm of the spectrum of shear has a variance of

$$\sigma_{\ln \Psi}^2 = \frac{5}{4} (N_f - N_V)^{-7/9} \quad (22)$$

419 (Lueck, 2022a). Thus, using coherent-noise removal to clean a shear spectrum not only biases the spectrum
420 low Eq. (21), but it also reduces its statistical reliability. The reduction of reliability is a consequence
421 of using information to identify and remove the coherent noise. The 95 % confidence interval of a shear
422 spectrum is

$$\Psi(k) \exp(\pm 1.96 \sigma_{\ln \Psi}) . \quad (23)$$

423 The values of $\sigma_{\ln \Psi}$, N_f and N_V , should appear in level L3 of the processed data file and they will be used
424 for quality control in level L4.

425 3.4 Level 4: Dissipation estimates from spectra

426 3.4.1 Estimating ε by spectral integration

427 A common method of estimating ε is by integrating the shear spectrum between a low and high
428 wavenumber limit. Particularly, the choice of the upper wavenumber limit of spectral integration must be
429 made after careful considerations described below. Estimating the variance of shear, and hence ε must be
430 done iteratively because the bandwidth required for an estimate, i.e., wavenumber limits of integration, is
431 *a priori* unknown since it depends on the value of ε itself. Very small dissipation rates $\lesssim 10^{-10} \text{ W kg}^{-1}$
432 are well resolved by a bandwidth of $\approx 10 \text{ cpm}$. Often vibrations and other sources of signal contamination
433 are small for wavenumbers smaller than $\approx 10 \text{ cpm}$. Thus, integrating a spectrum to 10 cpm can provide
434 an initial estimate of ε if the spectrum conforms reasonably closely to a model spectrum such as that by
435 Nasmyth (Fig. 3). The ratio of the actual dissipation rate, ε , to that estimated by integrating a spectral
436 model to only 10 cpm, ε_{10} , is well approximated by

$$\begin{aligned} \frac{\varepsilon}{\varepsilon_{10}} &= \sqrt{1 + a \varepsilon_{10}} + \exp(-b \varepsilon_{10}) - 1 \\ a &= 1.25 \times 10^{-9} \nu^{-3} \\ b &= 5.5 \times 10^{-8} \nu^{-5/2} \end{aligned} \quad (24)$$

437 (Fig. 6). The likely underestimated rate of dissipation, which is derived by integrating a measured (and
438 cleaned) spectrum to 10 cpm, can then be boosted by Eq. (24) to make an improved estimate of the rate
439 of dissipation, denoted ε_1 . According to most models, 95 % of the variance of shear is resolved at a
440 non-dimensional wavenumber of $\tilde{k}_{95} = 0.12$ (Fig. 3). Thus, $k_{95} = 0.12(\varepsilon_1/\nu^3)^{1/4}$, in units of cpm, is a
441 suitable upper limit for the integration of a shear spectrum. There is little point in integrating beyond this
442 wavenumber because the correction for the missing variance is only 5 %. If integrating to 10 cpm is not
443 convenient, then a boosting relationship such as Eq. (24) should be developed for other spectral limits to
444 derive an initial estimate of ε_1 .

445 Electronic noise sets another upper limit for spectral integration. Because of the differentiator operator
446 in obtaining shear, either done electronically in the signal chain or applied during post-processing of
447 the velocity time series, the noise in the spectrum of shear tends to rise with increasing wavenumber
448 (Fig. 2, down arrow). The wavenumber at which this spectral minimum occurs depends on ε . For very
449 low dissipation rates, the minimum occurs at low wavenumbers because the level of the spectrum rises in
450 proportion to $\varepsilon^{3/4}$, while the spectrum of electronic noise is constant at a given speed. For very high rates

of dissipation, the spectral minimum may not even appear because the electronic noise may be smaller than the shear signal at all wavenumbers. The spectrum of shear should not be integrated beyond the spectral minimum so that the estimate of the variance of shear is not biased high by electronic noise. The spectral minimum can be found by fitting a polynomial to the spectrum in log-log space. A fit of order 3 is often sufficient to find the spectral minimum but odd orders up to 7 also give satisfactory results. In most cases, the fit should be of an odd-numbered order because the typical shape of a spectrum, with respect to increasing wavenumber, is a rise from the lowest wavenumber to a peak, a subsequent decrease due to viscosity, and a final rise due to noise. This sort of shape is emulated by an odd-order polynomial. To avoid the detection of false minima, the minimum determined from a polynomial fit should not be smaller than 10 cpm because at this wavenumber a spectrum is about 95 % resolved when the rate of dissipation is very low, $\sim 10^{-10} \text{ W kg}^{-1}$. Let us denote the wavenumber of the spectral minimum by k_{\min} .

Another limit is due to the shear probe's limited wavenumber response (Eq. 18). We do not recommend integrating the spectrum beyond the wavenumber at which the spectral correction (for spatial averaging by the shear probe) exceeds a factor of 10. This is not a hard limit but spectra corrected by a factor much larger than 10 are unreliable because the correction itself has some uncertainty. We denote this limit due to spatial resolution by k_{SR} . It equals 150 cpm for the probes used by Macoun and Lueck (2004) and should be determined for other probes if they differ substantially from their probes.

Most data acquisition systems apply a low-pass filter to the continuous-domain shear signal before sampling to suppress aliasing. This is done in the continuous domain with a filter that has a cutoff frequency of f_{AA} . The spectrum is unresolved beyond this frequency. Therefore, another upper limit to spectral integration is $k_{AA} = 0.9 f_{AA}/W$ where the factor of 0.9 is used to avoid the transition from the pass band to the attenuation band of the anti-aliasing filter. This factor is suitable for an 8-th order Butterworth filter. Sharper filters can have a factor closer to unity, while filters of a lower order, or ones of a wider transition range, should use a factor that is smaller than 0.9.

Finally, there may be some corruption of the shear spectrum that is not removable but, if it is included in the spectral integration, it will bias high the estimate of the shear variance. This sort of spectral contamination is an instrument or an operational problem that should be corrected. If present, the contamination usually occurs at a (nearly) fixed frequency and, thus, this limit is usually specified in terms of frequency rather than wavenumber. If the spectrum is good for frequencies lower than f_{\lim} , then another limit of spectral integration, is $k_{\lim} = f_{\lim}/W$. For good data, f_{\lim} should be set to infinity so that it is irrelevant.

In summary, the various upper wavenumber limits of spectral integration are

- $k_{95} = 0.12(\varepsilon_1/\nu^3)^{1/4}$ – the wavenumber of 95 % resolution,
- k_{\min} – the wavenumber of the spectral minimum,
- k_{SR} – the wavenumber (typically 150 cpm) of the factor of 10 correction for spatial resolution,
- k_{AA} – the wavenumber corresponding to the cutoff frequency of the anti-aliasing filter, and
- k_{\lim} – the wavenumber of irremovable spectral corruption.

The spectrum of shear can now be integrated to estimate the variance of shear and to derive the second estimate of the rate of dissipation, ε_2 . For this estimate, the spectrum should be integrated to an upper limit equal to the smallest of the five cited upper limits. That is $k_u = \min(k_{95}, k_{\min}, k_{\text{SR}}, k_{AA}, k_{\lim})$. The upper limit k_u will usually be larger than 10 cpm and, therefore, the estimate ε_2 derived by integration to k_u will be statistically more reliable than the initial estimate, ε_1 . However, the spectrum is not fully resolved at k_u and ε_2 will be an underestimate because some shear variance will be excluded.

493 The estimated ε_2 is then used to estimate the non-dimensional value of the upper wavenumber of spectral
 494 integration, namely

$$\tilde{k}_u = k_u (\nu^3 / \varepsilon_2)^{1/4} . \quad (25)$$

495 This value is used with one of the models of the integral of a spectrum (Eq. 11) to estimate the fraction of
 496 the shear variance that is resolved by integrating the spectrum to k_u . For example, the resolved fraction is
 497 $I_L(\tilde{k}_u)$, and an improved estimate is

$$\varepsilon_3 = \varepsilon_2 / I_L(k_u [\nu^3 / \varepsilon_2]^{1/4}) \quad (26)$$

498 and this should be followed by

$$\varepsilon_4 = \varepsilon_3 / I_L(k_u [\nu^3 / \varepsilon_3]^{1/4}) \quad (27)$$

499 and repeated until the increases of ε become smaller than 1 %. For spectra with an upper limit, k_u , that
 500 is higher than the wavenumber of the peak of the spectrum, this iteration converges in one or two cycles,
 501 because of the $\varepsilon^{1/4}$ dependence of the non-dimensional wavenumber. Even for upper limits that are smaller
 502 than the peak wavenumber, the dissipation estimates converge quickly and they agree (on average) with
 503 estimates that use the same spectrum but have wavenumber limits beyond the peak wavenumber. This can
 504 be verified by imposing a k_{lim} to lower than the upper wavenumber when such a limitation is not required.

505 When integrating the spectrum from a wavenumber of zero, the spectral value at zero wavenumber should
 506 be forced to zero because that is the expectation of the spectrum. Algorithms that estimate the variance of
 507 shear by integrating the spectrum from the lowest non-zero wavenumber, k_l , have to correct their estimate
 508 for the exclusion of variance below their lower limit of spectral integration and this can be done with a
 509 model such as (Eq. 11).

510 The integration of the spectrum is usually done by the trapezoidal approximation of an integral. This
 511 introduces a slight error in the low wavenumber range. The spectrum is expected to rise as $k^{1/3}$ from
 512 a wavenumber of zero to at least the first non-zero wavenumber, k_1 . This makes the integral equal to
 513 $3 k_1 \Psi(k_1)/4$. However, the trapezoidal approximation gives $k_1 \Psi(k_1)/2$ which is smaller than a true
 514 integral. An amount equal to $k_1 \Psi(k_1)/4$ should be added to the estimated variance to correct this shortfall.

515 3.4.2 Estimating ε by fitting to the inertial subrange

516 When dissipation rates are very high, $\varepsilon \gtrsim 10^{-5} \text{ W kg}^{-1}$, the shear probe cannot resolve the spectrum
 517 of shear and even the wavenumber correction proposed by Macoun and Lueck (2004) does not produce
 518 spectra that agree well with spectral models. However, the shear probe always resolves the inertial subrange,
 519 for oceanic conditions, which has wavenumbers smaller than $k < 0.01 (\varepsilon / \nu^3)^{1/4}$ in units of cpm, and
 520 this range can be estimated with the value of ε_1 derived from the spectral integration to 10 cpm. Fitting
 521 the spectrum in the inertial subrange provides an alternative method to spectral integration. The model
 522 spectrum in the inertial subrange is given by Eq.(12).

523 The actual fitting method is not crucial. One method that gives satisfactory results is to use ε_1 (derived
 524 from a spectral integration to 10 cpm) to delineate the inertial subrange. The ratio of the observed and
 525 model spectral values is then computed and averaged over the subrange. The rate of dissipation of the
 526 model spectrum (Eq. 12) is adjusted until the average ratio equals unity (to within, say, 1 %). This method
 527 is the same as log-transforming the inertial subrange model and solving this relation

$$\ln \Psi(k) - \ln A - \frac{1}{3} \ln k = \ln \varepsilon^{2/3} \quad (28)$$

528 over the inertial subrange, where $\Psi(k)$ is the observed spectral observations.

529 The number of spectral values used for a dissipation estimate by a fit to the inertial subrange is almost
 530 always smaller than the number of values used in spectral integration. Consequently, the statistical reliability
 531 of such an estimate is inferior to that obtained by integration.

532 3.4.3 Uncertainty of an ε estimate by spectral integration

533 The statistical reliability of an estimate of the dissipation rate has been explored by Lueck (2022b).
 534 Uncertainty of an ε estimate is different for methods of spectral integration and fitting in the inertial
 535 subrange and must be carefully calculated. When the rate of dissipation is estimated by spectral integration,
 536 the statistical uncertainty of such an estimate has a variance of

$$\sigma_{\ln \varepsilon}^2 = \frac{5.5}{1 + (\hat{L}_f/4)^{7/9}}, \quad \hat{L}_f = \hat{L} V_f^{3/4} = \frac{L}{L_K} V_f^{3/4}, \quad (29)$$

537 where L is the length (in units of m) of data used for the dissipation estimate, $L_K = (\nu^3/\varepsilon)^{1/4}$ is the
 538 Kolmogorov length, and V_f is the fraction of the shear variance resolved by ending the spectral integration
 539 at a finite wavenumber of k_u (Lueck, 2022b). The non-dimensional data length, \hat{L}_f , is reduced by a factor
 540 of 4 because samples of shear are independent only if they are separated by more than four Kolmogorov
 541 lengths, where the lagged auto-correlation of shear drops to one-half Lueck (2022b). The factor of V_f
 542 accounts for the underusage of information because of limiting the spectral integration to $k \leq k_u$. Thus,
 543 the 95 % confidence interval for a dissipation estimate derived by spectral integration is

$$\varepsilon \exp(\pm 1.96 \sigma_{\ln \varepsilon}) . \quad (30)$$

544 In level L4, every estimate of ε should be accompanied by its value $\sigma_{\ln \varepsilon}$, L , L_K , and V_f , if the estimate
 545 was made by spectral integration, as explained in Sec. 3.4.1.

546 3.4.4 Uncertainty of an ε estimate by fitting in the inertial subrange

547 The method of fitting a spectrum in the inertial subrange to a model spectrum is equivalent to finding the
 548 average of Eq.(28) for the spectral values in the inertial subrange. The logarithm of each spectral value has
 549 a variance of Eq.(22). If there are N_{isr} spectral values in the inertial subrange, the variance of the average
 550 logarithmic differences is smaller by a factor of N_{isr} . Thus, the 95 % confidence interval of $\ln(\varepsilon^{2/3})$ is

$$\ln(\varepsilon^{2/3}) \pm 1.96 \frac{\sigma_{\ln \Psi}}{\sqrt{N_{\text{isr}}}} \quad (31)$$

551 and the same confidence interval for ε itself is

$$\varepsilon \exp\left(\pm 1.96 \frac{3}{2} \frac{\sigma_{\ln \Psi}}{\sqrt{N_{\text{isr}}}}\right) . \quad (32)$$

552 In level L4, every estimate of ε derived by fitting in the inertial subrange should be accompanied by its
 553 value of N_{isr} , so that one can place a confidence interval on this estimate using Eq. 32 and the value of
 554 $\sigma_{\ln \Psi}$ that is located in level L3 (Sec. 3.3.5).

555 3.4.5 Quality Assurance Metrics

556 The quality of a dissipation estimate, and the spectrum from which it is derived, must be quantified and
 557 must accompany each estimate. The quality-control metrics can be combined into a single Q flag value that
 558 is a combination of bitwise flags with boolean values. A value of $Q = 0$ means that the estimate passed all
 559 metrics. Failures increase the value of Q by the amounts described below.

560 Poor figure of merit ($Q = 1$)

561 Figure of merit (FOM) is a measure of the quality of a spectrum, over the range of wavenumbers that is
 562 used for the estimation of ε . The variance of a spectral estimate is given by (Eq. 22) and, if there are N_s
 563 spectral values in the wavenumber range used to make a dissipation estimate (excluding the wavenumber
 564 $k = 0$), the mean absolute deviation ($MAD_{\ln \Psi}$) of the logarithm of the spectral values from the logarithm
 565 of a reference spectrum should not exceed

$$\sigma_{\ln \Psi} T_M = \sigma_{\ln \Psi} \left(0.8 + \frac{1.25}{\sqrt{N_s}} \right), \quad (33)$$

566 for 97.5% of the estimates that are based on N_s spectral values. The factor T_M is determined from a
 567 sampling of a normal process with a standard deviation of 1 (Fig. 7). We obtain

$$FOM = \frac{MAD_{\ln \Psi}}{\sigma_{\ln \Psi}} \frac{1}{T_M}, \quad (34)$$

568 and FOM should be smaller than 1 for 97.5% of the spectra. The various spectral models differ by about
 569 15 % and, therefore, an appropriate cutoff for rejection might be $FOM \gtrsim 1.15$. In level L4, every estimate
 570 of ε should be accompanied by its value of FOM, $MAD_{\ln \Psi}$ and N_s . The flag value of estimates with poor
 571 FOM must be increased by a value of 1.

572 Large fraction of data with spikes ($Q = 2$)

573 The fraction of the data that was modified for extrema removal (Sec. 3.2.2), for each section of data used
 574 for a dissipation estimate, should be noted. There are currently no standards for an acceptable fraction.
 575 Nonetheless, estimates that are based on data that has more than a few percent of modification should be
 576 treated with caution. We recommend that a fraction larger than 5 % be flagged and that Q be increased by a
 577 value of 2.

578 Large disagreement between dissipation estimates from probes ($Q = 4$)

579 Simultaneous dissipation estimates from two or more probes will never agree exactly, and the statistical
 580 uncertainty of an ε estimate can be used to flag, and possibly reject, one of the estimates. Signal
 581 contamination will bias an estimate high by adding variance. Thus, it is the larger of a pair of estimates that
 582 should be rejected, if their ratio is excessive. The geometric mean of a pair of dissipation estimates derived
 583 by spectral integration has a 95 % confidence interval of

$$\sqrt{\varepsilon_1 \varepsilon_2} \exp \left(\pm 1.96 \sigma_{\ln \varepsilon} \sqrt{1/2} \right) \quad (35)$$

584 where the factor of $\sqrt{1/2}$ accounts for the one degree of freedom consumed in calculating the geometric
 585 mean. Thus, there is only a 5 % chance that the ratio of two estimates falls outside of the interval

$$\exp \left(\pm 1.96 \sigma_{\ln \varepsilon} \sqrt{2} \right) \quad (36)$$

586 when they are derived by spectral integration, and that their ratio falls outside of the interval

$$\exp \left(\pm 1.96 \frac{3}{2} \sqrt{2} \frac{\sigma_{\ln \Psi}}{\sqrt{N_{\text{isr}}}} \right) \quad (37)$$

587 if they are derived from fitting in the inertial subrange. That is, the magnitude of the difference of
 588 the logarithm of two dissipation estimates should be smaller than $1.96\sqrt{2}\sigma_{\ln \varepsilon}$, which equals $2.77\sigma_{\ln \varepsilon}$,
 589 and smaller than $1.96 \frac{3}{2} \sqrt{2} \sigma_{\ln \Psi} / \sqrt{N_{\text{isr}}}$, which equals $4.2 \sigma_{\ln \Psi} / \sqrt{N_{\text{isr}}}$, if they are derived by spectral
 590 integration and fitting to the inertial subrange, respectively. Quality assurance requires that the values of
 591 $\sigma_{\ln \varepsilon}$, $\sigma_{\ln \Psi}$, and N_{isr} be provided with every estimate of the rate of dissipation. Dissipation estimates that
 592 are larger than the other simultaneous estimates must be flagged and Q must be increased by a value of 4.

593 *Too many iterations of de-spiking routine ($Q = 8$)*

594 While the fraction of the data altered by a de-spiking routine must be examined for each data segment used
 595 to estimate a spectrum of shear ($Q = 2$), the number of iterations made to clean the shear-probe data of
 596 level L2 is a quality-control metric that applies to the entire section. We recommend that the entire section
 597 of dissipation estimates requiring more than 8 passes of the de-spiking routine must be flagged and Q
 598 must be increased by a value of 8. It is important to apply the de-spiking routine to the selected section as
 599 described in Section 3.2.1.

600 *Insufficient variance resolved ($Q = 16$)*

601 We recommend that the fraction of variance resolved, V_f , must exceed 0.5 for both (isr or vsr) methods of
 602 dissipation rate estimation. Estimates failing this criterion must be flagged and Q must be increased by a
 603 value of 16.

604 Flag values of 32, 64, and 128 are reserved for manual flags identified by the user. The various quality
 605 control metrics should be combined into a single “flag” value for each dissipation estimate from each probe.
 606 For example $Q = 20$ means that the dissipation estimated failed both the dissipation ratio limit test and the
 607 resolved variance test, or $Q = 3$ means poor FOM and a large fraction of de-spiked data. When there is
 608 more than a single probe providing good dissipation estimates ($Q = 0$), they can be averaged to provide
 609 the final dissipation estimate.

4 BENCHMARK DATA

610 4.1 Example of good data

611 In ATOMIX, we have identified and tested a collection of five benchmark shear-probe datasets from
612 different platforms. These benchmarks, described in Fer et al. (in preparation), demonstrate a variety of
613 aspects of the estimation of dissipation rates. The datasets are presented in a well-defined and homogeneous
614 format that encompasses all levels from L1 to L4. These datasets provide a resource for users to evaluate
615 their routines and allow for platform-independent analysis of shear probe data once the Level 1 data is
616 provided. Users can then analyze data from their desired level, such as starting with Level 1, selecting
617 sections of cleaned time series from Level 2, or utilizing corrected shear spectra from Level 3. Here, we
618 present an example of our best practices recommendations using one benchmark dataset and direct readers
619 to Fer et al. (in preparation) for a comprehensive overview. The example profile including all four levels,
620 can be obtained from (Fer, 2023).

621 The example dissipation profile is from the Faroe Bank Channel overflow. The bottom-attached overflow
622 plume of dense, cold water exhibits energetic turbulence and is described in detail in Fer et al. (2010,
623 2014). The profile was collected using the tethered free-fall vertical microstructure profiler (VMP, model
624 VMP2000, SN 009, Rockland Scientific, Canada) on 10 June 2012 from the Research Vessel *Haakon*
625 *Mosby*. The water depth is about 860 m. The dissipation rate was measured using two orthogonal shear
626 probes. Other sensors on the instrument were a fast-response FP07 thermistor, a Sea-Bird Electronics
627 (SBE) microconductivity sensor, a 3-axis accelerometer, a magnetometer, and a pumped SBE conductivity-
628 temperature package. The turbulence sensors were protected by a probe guard. The VMP sampled the signal
629 plus signal derivative on the thermistor, microconductivity, and pressure transducer, and the derivative
630 for shear signals. The turbulence and acceleration channels were sampled at a rate of 512 Hz, while the
631 other channels were sampled at 64 Hz. Data were transmitted to a shipboard data acquisition system. The
632 instrument was deployed from the side of the vessel (drifting away from the profiler) using a hydraulic
633 winch with a line-puller system, allowing it to fall freely at a nominal fall rate of about 0.6 m s^{-1} .

634 When preparing the Level 2 time series, the shear probe and accelerometer time series are high-pass
635 filtered using a cutoff frequency of 0.25 Hz, which corresponds to one-half of the inverse of the FFT
636 length (Eq. 17) that is used for the analysis in Level 3. The shear data are cleaned, following the method
637 of Sec. 3.2.2, using a first-order, low-pass, Butterworth filter with a cutoff frequency of 0.5 Hz and a
638 threshold of 8. The fall rate, W is calculated from the rate of change of pressure and smoothed with a
639 low-pass filter with a cut-off frequency of 0.5 Hz that was applied both forwards and backwards. A section
640 is extracted from the record when W was larger than 0.4 m s^{-1} (80 % of estimated minimum fall rate) and
641 when the depth exceeded 10 m to avoid ship effects. At the typical fall rate, high-pass filtering applied
642 in Level 2 will suppress the signals at vertical scales larger than the profiler length of about 2 m. Shear
643 spectra are estimated using record lengths of 8 s and FFT lengths of 2 s that are cosine windowed and
644 overlapped by 50 %, resulting in $N_f = 7$. Vibration-coherent noise is removed using the records from
645 all three accelerometers ($N_V = 3$) with the method of Goodman et al. (2006). The frequency spectra are
646 converted to wavenumber spectra using the average fall rate for each spectrum. The rate of dissipation is
647 estimated by spectral integration (Sec. 3.4.1). Successive dissipation estimates are overlapped by 50 % (i.e.,
648 about 2.5 m vertical resolution using 8 s record length at 0.6 m s^{-1}).

649 Time series of selected parameters are shown in Fig. 8 for the entire record. Early in the record, the
650 profiler accelerates to its free fall velocity, which is approximately 0.6 m s^{-1} , and stops falling after about
651 1400 s when the cable is taut. The section chosen for analysis is approximately between 10 s and 1400 s,

marked by arrows. Note that only the extracted section is de-spiked and prepared for spectral analysis. Near about 600 dbar, a strong eddy above the turbulent dense bottom current disturbs the fall rate, a slight decrease followed by downdraught. Shear probe (Fig. 8b-c) and horizontal acceleration (Fig. 8d-e) records from Level 1 are shown in blue and the corresponding records of Level 2 that are high-pass filtered and de-spiked in red, with offset. We see that short, spiky segments of shear (blue) are removed successfully in Level 2 (red, note the shear axes are restricted and some outliers reach much larger values). Relatively low-frequency signals in the accelerometer records of Level 1 (blue) are at vertical scales comparable to and larger than the instrument length and are filtered out in Level 2 (red).

Dissipation estimates from both probes agree within their expected statistical uncertainty (Eq. 36), and their values span a range of 4 factors of 10 (Fig. 9b). All estimates are smaller than $1 \times 10^{-5} \text{ W kg}^{-1}$ and, therefore, they were obtained using the spectral integration method. Most estimates are of high quality and pass the quality control (QC) tests. Those that fail do so because they exceed the FOM criterion (the threshold was set to 1.15 in Eq. 34). The final dissipation estimate is typically the average of the estimates from both probes. When the estimate from one of the probes fails the QC tests, the final estimate comes from the other probe. When both probes fail the QC test, which occurred for a few estimates near 100 and 600 dbar, no value is reported for that depth (time) range.

We select example spectra from three segments with low, moderate, and high dissipation rates (Fig. 10a-c, respectively), all of which pass the QC (Sec. 3.4.5), and another segment when both probes fail (Fig. 10d). All spectra show a well-identified minimum varying between 20 cpm and 80 cpm. At higher wavenumbers the spectra are dominated by electronic noise. The average pressure, estimated dissipation rates and FOM for the spectra are listed in Table 1.

As an example, we made alternative estimates of ε using the method of fitting to the inertial subrange (Sec. 3.4.2), to demonstrate the limitations of this method for $\varepsilon < 10^{-5} \text{ W kg}^{-1}$. Resulting estimates are listed in Table 1 together with the estimates from the integration method in the viscous subrange. For the quiescent spectrum ($\varepsilon \approx 1 \times 10^{-9} \text{ W kg}^{-1}$, Fig. 10a), only 3 spectral points are within the inertial subrange of $k \leq 0.01(\varepsilon/\nu^3)^{1/4}$ (actually only 2, because our software forces inertial subrange estimates to use at least 3 points). Comparing the three marked spectra points (Fig. 10a) against the reference spectrum (grey) shows that an estimate using the inertial subrange would produce a large underestimate for probe 1 (thick blue) but provide a reasonable estimate for probe 2 (thick red). For energetic spectra, the inertial subrange contains many points, and an estimate of ε by fitting in this range produces more reliable estimates compared to estimates for low dissipation rates. For example, ten spectral points fall within the inertial subrange in (Fig. 10c) ($\varepsilon = 1.5 \times 10^{-7} \text{ W kg}^{-1}$). Comparing the level of these points to the reference spectrum (gray) indicates that the inertial subrange estimates from both probes will agree closely with the estimates obtained by spectral integration. Thus, we recommend using the inertial subrange method only when dissipation rates are high, $\varepsilon \gtrsim 10^{-5} \text{ W kg}^{-1}$.

4.2 Example of poor data

Many things can go wrong while collecting turbulence data with shear probes. The nonuniform speed of profiling is a common occurrence that can severely compromise the quality of the data reported by the shear probe. Tethered instruments must be attached to a line that is paid out rapidly enough to continuously maintain slack so that the profiler is decoupled from the motions of the deployment platform and descends smoothly throughout its profile. Sometimes, the loose tether snags, and the smooth profiling is interrupted.

The profile shown in Fig. 11 was collected with a VMP-250 that was deployed from a small inflatable dive-boat in the Agulhas Current about 1 km offshore Sodwana Bay, South Africa, where the current speed

695 exceeds 1 m s^{-1} . The speed of the profiler was nearly double above its normal value to reduce its drift away
 696 from the boat, and to reduce the angle of attack on the shear probes due to the anticipated large rates of
 697 dissipation. Pairs of profiles were collected at each station. The fall rate of the instrument was nominal
 698 during its first profile (Fig. 11a, blue), but the tether snagged on dive gear during the second profile (red).
 699 The profiler slowed its descent near 55, 193, 229, and 248 dbar. The middle two of these four interruptions
 700 jerked the profiler significantly (Fig. 11 c), which also induced a large anomaly in the shear-probe signals
 701 (panel d). In fact, the jerk was so large that it drove the sampler of the vibration sensor into negative
 702 saturation (-2^{15}). (The vibration sensors are not calibrated and their signals are not converted into physical
 703 units because this is not necessary). Thus, even if problems with the deployment of the tether do not cause
 704 a profiler to stop descending, there can still be considerable contamination of the shear-probe signals.

705 Shear spectra were computed for the second profile using data lengths of 5 s and FFT lengths of 0.5 s,
 706 that were cosine tapered and overlapped by 50 %. Both vibration sensors were used to remove vibration-
 707 coherent noise from the shear-probe spectra. From Eq. 22, the standard deviation of the logarithm of the
 708 spectral values is

$$\sigma_{\ln \Psi} = \sqrt{\frac{5}{4} (N_f - N_V)^{-7/9}} = \sqrt{\frac{5}{4} (19 - 2)^{-7/9}} = 0.37, \quad (38)$$

709 where $N_f = 19$ is the number of FFT segments used for the estimate and $N_V = 2$ is the number of
 710 vibration signals that were used to remove vibration-coherent noise. Using Eq. 23, the 95 % confidence
 711 interval for the spectral values is

$$\text{CI}_{95} = \exp(\pm 1.95 \sigma_{\ln \Psi}) = [2.07, 0.48]. \quad (39)$$

712 Spectra from a depth range free of fall-rate anomalies follow the model spectrum quite well (Fig. 12 a).
 713 The expected spectrum (gray) is well centered on the 95 % confidence intervals of the spectra (blue and
 714 red shading). However, for both shear probes, their spectra for the region near to 193 dbar depart far from
 715 their expectation (Fig. 12 b). Their FOM is much larger than one and more than 5 % of the data for these
 716 spectra have been modified by the de-spiking routine. The estimated dissipation rates must be rejected both
 717 because of the poor quality of the spectra ($\text{FOM} \gg 1$) and because of the larger fraction of the data that
 718 was modified by the de-spiking routine ($\gtrsim 1\%$).

719 A de-spiking routine can often effectively remove shear anomalies due to collisions with zooplankton.
 720 However, a strong jerking of the profiler by its tether is only partially ameliorated (Fig. 13 blue versus red).
 721 Similar results were obtained for the de-spiking of shear probe 2. The anomalies are reduced but the data
 722 are still not usable.

5 DISCUSSION

723 The ATOMIX approach described here consolidates knowledge of methods of estimating ε from shear-
724 probe turbulence measurements while developing best practices and quality-control metrics for determining
725 ε . From the outset, the Working Group sought to produce recommendations that are applicable to a range
726 of commonly deployed platforms. This was achieved by gathering researchers from different sub-fields
727 which brought together different experiences in terms of application and scale.

728 As the best practices and quality-control metrics were developed, it became apparent that the scientific
729 questions and scales for the particular study are key considerations for processing. Most of the flexibility
730 in processing choices is in level L3 of the workflow. We strongly recommend the Level 1 and Level 2
731 steps described above. Our recommended procedure for removing spikes from shear-probe data performs
732 well in typical conditions and is routinely used by most of the ATOMIX shear-probe group. There are
733 different methodologies for de-spiking high-frequency resolution data, such as shear-probe signals, and
734 an experienced user can assess whether an alternative method (e.g., using de-spiking based on nonlinear
735 filtering) performs better for a particular dataset. In any case, we strongly recommend that the effect of
736 de-spiking, such as the number of despiking passes applied, the fraction of the time series removed, etc., be
737 documented as quality control parameters.

738 Two of the major choices in the workflow that are directly connected to the particular scientific questions
739 are the choice of data length for a dissipation estimate and the length of the FFT segments for this estimate.
740 In some applications such as boundary layer profiling or thermocline studies, there will be a natural desire
741 to use short data lengths for dissipation estimation in order to maximize the spatial resolution of the
742 estimates. In these situations, we advise caution because the low statistical reliability of the spectra impacts
743 the uncertainty of the epsilon estimate. The researchers will need to evaluate and justify the trade-offs
744 in each particular situation such as statistical reliability versus spatial resolution and the number of FFT
745 segments.

746 The use of vibration-coherent noise removal is also strongly advised. Coherent noise removal increases
747 the comparability of dissipation estimates across different platforms. Additionally, low-noise instruments
748 may exhibit elevated shear contributions from platform vibrations in elevated turbulence regimes. An
749 example of such data is provided in Fer et al. (in preparation) (ref: VPM250_TidalChannel_24, also
750 accessible from the ATOMIX wiki site), where shear signal contributions from platform vibrations lead to
751 estimates of dissipation rates enhanced by more than a factor 3 in regions where dissipation rates exceed
752 $10^{-5} \text{ W kg}^{-1}$. We recommend the method of Goodman et al. (2006), particularly because the bias due to
753 the statistical loss of variance inherent to the method, which may have discouraged researchers from using
754 the method in the past, can now be corrected (Ferron et al., 2023).

755 Clearly, the Best Practices approach can be utilised in a number of ways. For researchers and students new
756 to the field it offers a general primer to ocean turbulence measurement using shear probes. For practitioners,
757 it provides a synthesis of peer-developed recommendations as a shortcut to evaluate and improve their
758 measurements. Finally, for turbulence researchers it provides a baseline from which to identify and improve
759 gaps in the approaches. Furthermore, by homogenizing the data format and parameter names as described
760 in the ATOMIX wiki and Fer et al. (in preparation), reprocessing the data with the user's own routines and
761 attempting to reproduce scientific results are better streamlined.

762 The wider ATOMIX methodology systematically considers three different approaches to turbulence
763 quantification in parallel developments - the other two being Acoustic Doppler Current Profiler and

764 Acoustic Doppler Velocimetry. This consistent parallel approach provides a bridge for researchers in that
765 they can more readily shift between techniques that best suit their application.

766 ATOMIX was motivated to engage with the ocean turbulence community on a number of levels. Firstly,
767 there is a need to grow the community so that more researchers have a deeper knowledge of the measurement
768 possibilities, limitations, and pitfalls. Secondly, any development will necessarily come from a limited set
769 of perspectives. The advancement of the field requires a way to engage with new researchers, techniques,
770 applications, and platforms.

771 One of the new applications the turbulence community is approaching relies on the integration of
772 turbulence sensors onto autonomous platforms. Such integration already exists for platforms like ocean
773 gliders and autonomous underwater vehicles (AUVs), but until recently, the data processing and the
774 computation of turbulent dissipation rates were done after the deployment. This requires the platform's
775 recovery and limits the length of the deployments. The progress made over the last decade in micro-
776 electronics allows the development of microprocessors capable of handling the amount of data necessary
777 to process onboard the turbulent dissipation rates (e.g., Hughes et al. 2023). The onboard processing
778 dramatically reduces the amount of data an instrument must store to provide ϵ and offers the possibility of
779 transferring turbulence data via low-bandwidth links, such as satellite communications. A platform with
780 onboard processing and satellite communication capabilities should be able to sample the ocean over a few
781 months or years, provided that the probes' resilience and the battery capacity allow it.

782 The gain in memory space and the data compression associated with the onboard processing comes with
783 a caveat: The quality of the data must be assessed during the processing, and quality flags accepted by the
784 whole community should be published with the data. The present paper provides an accepted methodology
785 and quality flags that are based on the statistical nature of turbulence measurements and are agreed upon by
786 the ATOMIX Working Group, using three different types of microstructure sensors and different types of
787 platforms. Such a consensus is one of the necessary steps toward global, consistent and perennial turbulence
788 observation programs.

789 In a changing climate where the oceans are warming, it is vital that global ocean monitoring continues to
790 evolve. The flagship Argo program (Roemmich et al., 1999) recently identified the observation of turbulent
791 mixing as one of its developing branches (Roemmich et al., 2019). A handful of successful prototypes
792 of Argo-floats equipped with microstructure sensors have already been tested, paving the way for longer
793 deployments. A successful integration of microstructure sensors on these Argo floats would provide for
794 the first time a systemic approach to turbulence measurement and is pushing the turbulence community to
795 scale up the management of the turbulence data as well as the production of these sensors.

796 In an effort to coordinate such evolution, and largely based upon the SCOR Working Group effort
797 presented here, the ocean mixing community is working with the Global Ocean Observing System steering
798 committee to get the turbulent diapycnal fluxes computed from ϵ registered officially has an essential ocean
799 variable (Sloyan et al., 2019). With the growing need for ocean health monitoring, the expectation is that
800 this best practices work will be revisited, updated, and extended relatively soon.

6 CONCLUSIONS

801 There is an increasing interest and availability of instruments and platforms using shear probes. The
802 spectrum of expertise of users spanning from operators through scientists, as well as the peer reviewers
803 of the scientific productions, is broad. The community will benefit from guidelines and best practices
804 for dissipation estimates, and a relatively streamlined structure of processing steps and dataset formats.
805 The shear-probes team of the SCOR Working Group on "Analysing ocean turbulence observations to
806 quantify mixing" (ATOMIX), aims to take the first step in consolidating knowledge and offering best
807 practices and quality-control metrics for methods of estimating dissipation rates from measurements of
808 shear probes. It is crucial to make informed choices of data processing parameters and be familiar with
809 the limitations of the platforms, the probes, and the data processing choices that reflect on the dissipation
810 estimates. In future studies using dissipation estimates from shear probe data, we strongly recommend
811 the researchers test their method and algorithm against benchmark datasets to gain confidence in their
812 estimates. The reproducibility of dissipation estimates is only possible when the archived data accessible to
813 users have all the required and necessary parameters together with a minimum of L1 time series records
814 with the dissipation estimates. We highly recommend archiving data with all four levels of processing
815 described here. Our recommendations are applicable to commonly deployed platforms and will facilitate
816 the reproducibility of dissipation estimates and their interpretation. As ocean monitoring continues to
817 evolve, we expect that this best practices work will be updated and extended. A desired and necessary
818 extension is the development of such best practices for the turbulent dissipation rate of temperature gradient
819 χ .

CONFLICT OF INTEREST STATEMENT

820 The authors declare that they do not have any commercial or financial relationships that could be construed
821 as a potential conflict of interest.

AUTHOR CONTRIBUTIONS

822 The content of the manuscript is initiated and developed by the shear probe group members of the ATOMIX.
823 RL drafted the paper and produced most of the figures; IF restructured the first draft, processed the
824 benchmark data, and wrote the relevant section with figures; KS prepared the flow chart; all authors
825 commented on the manuscript and tested the benchmark data.

FUNDING

826 This manuscript is based on work conducted by the Scientific Committee on Oceanic Research (SCOR)
827 Working Group 160: "Analysing ocean turbulence observations to quantify mixing" (ATOMIX). SCOR
828 Working Group 160 is funded by the NSF grant to SCOR OCE-2140395 as well as by contributions from
829 the national SCOR committees.

ACKNOWLEDGMENTS

830 The authors wish to express their never-ending gratitude to the ocean microstructure research community
831 for its unwavering support and encouragement during the grueling task of developing some sort of sensible
832 guidelines for processing aquatic shear-probe data. We thank the other members of the ATOMIX Working
833 Group and the external experts we approached for their comments.

DATA AVAILABILITY STATEMENT

834 The benchmark dataset discussed here can be found at NERC EDS British Oceanographic Data Centre
835 NOC, <http://doi.org/10.5285/05f21d1d-bf9c-5549-e063-6c86abc0b846>.

REFERENCES

- 836 Allen, H. J. and Perkins, E. W. (1951). *A study of effects of viscosity on flow over slender inclined bodies*
837 *of revolution*. Report 1048, National Advisory Committee for Aeronautics
- 838 Antoniou, A. (1979). *Digital Filters: Analysis and Design* (McGraw-Hill)
- 839 [Dataset] Fer, I. (2023). ATOMIX shear probes benchmark data: a dissipation profile from the Faroe
840 Bank Channel overflow obtained by a vertical microstructure profiler in June 2012. NERC EDS British
841 Oceanographic Data Centre NOC. doi:10.5285/05f21d1d-bf9c-5549-e063-6c86abc0b846
- 842 Fer, I. and Bakhoday Paskyabi, M. (2014). Autonomous ocean turbulence measurements using shear probes
843 on a moored instrument. *J. Atmos. Ocean. Technol.* 31, 474–490. doi:10.1175/JTECH-D-13-00096.1
- 844 Fer, I., Dengler, M., Holtermann, P., Inoue, R., Le Boyer, A., and Lueck, R. (in preparation). ATOMIX
845 Shear Probe Benchmark Datasets. *Scientific Data*
- 846 Fer, I., Peterson, A. K., and Ullgren, J. E. (2014). Microstructure measurements from an underwater glider
847 in the turbulent Faroe Bank Channel overflow. *Journal of Atmospheric and Oceanic Technology* 31,
848 1128–1150. doi:10.1175/JTECH-D-13-00221.1
- 849 Fer, I., Voet, G., Seim, K. S., Rudels, B., and Latarius, K. (2010). Intense mixing of the Faroe Bank
850 Channel overflow. *Geophys. Res. Lett.* 37, L02604. doi:10.1029/2009gl041924
- 851 Ferron, B., Bouruet Aubertot, P., Cuypers, Y., and Vic, C. (2023). Removing biases in oceanic turbulent
852 kinetic energy dissipation rate estimated from microstructure shear data. *Journal of Atmospheric and*
853 *Oceanic Technology* 40, 129–139. doi:10.1175/JTECH-D-22-0035.1
- 854 Fleury, M. and Lueck, R. G. (1992). Microstructure in and around a double-diffusive interface. *Journal of*
855 *Physical Oceanography* 22, 701–718. doi:10.1175/1520-0485(1992)
- 856 Frajka-Williams, E., Brearley, J. A., Nash, J. D., and Whalen, C. B. (2022). Chapter 14 - New technological
857 frontiers in ocean mixing. In *Ocean Mixing*, eds. M. Meredith and A. N. Garabato (Elsevier). 345–361.
858 doi:10.1016/B978-0-12-821512-8.00021-9
- 859 Goodman, L., Levine, E. R., and Lueck, R. G. (2006). On measuring the terms of the turbulent kinetic
860 energy budget from an auv. *Journal of Atmospheric and Oceanic Technology* 23, 977–990. doi:10.1175/
861 JTECH1889.1
- 862 Gregg, M. C. (2021). *Ocean Mixing* (Cambridge: Cambridge University Press). doi:10.1017/
863 9781316795439
- 864 Hughes, K. G., Moum, J. N., and Rudnick, D. L. (2023). A turbulence data reduction scheme for
865 autonomous and expendable profiling floats. *Ocean Science* 19, 193–207
- 866 Kolmogorov, A. N. (1941). Local structure of turbulence in an incompressible fluid at very high Reynolds
867 number. *Doklady AN SSSR* 4, 299–303
- 868 Lueck, R. (2022a). The statistics of oceanic turbulence measurements. Part 2: Shear spectra and a
869 new spectral model. *Journal of Atmospheric and Oceanic Technology* 39, 1273–1282. doi:10.1175/
870 JTECH-D-21-0050.1.
- 871 Lueck, R. G. (2022b). The statistics of oceanic turbulence measurements. Part 1: Shear variance and
872 dissipation rates. *Journal of Atmospheric and Oceanic Technology* 39, 1259–1271. doi:10.1175/
873 JTECH-D-21-0051.1.
- 874 Macoun, P. and Lueck, R. (2004). Modelling the spatial response of the airfoil shear probe using
875 different sized probes. *Journal of Atmospheric and Oceanic Technology* 21, 284–297. doi:10.1175/
876 1520-0426(2004)021
- 877 McMillan, J. M., Hay, A. E., Lueck, R. G., and Wolk, F. (2016). Rates of Dissipation of Turbulent Kinetic
878 Energy in a High Reynolds Number Tidal Channel. *Journal of Atmospheric and Oceanic Technology* 33,
879 817–837. doi:10.1175/JTECH-D-15-0167.1

- 880 Moum, J. N., Gregg, M. C., Lien, R. C., and Carr, M. E. (1995). Comparison of turbulence kinetic energy
881 dissipation rate estimates from two ocean microstructure profilers. *Journal of Atmospheric and Oceanic
882 Technology* 12, 346–366
- 883 Nagai, T., Inoue, R., and Yamazaki, A. T. H. (2015). Evidence of enhanced double-diffusive convection
884 below the main stream of the kuroshio extension. *Journal of Geophysical Research – Oceans* 120,
885 8402–8421. doi:10.1002/2015JC011288
- 886 Nasmyth, P. W. (1970). *Ocean Turbulence*. Ph.D. thesis, University of British Columbia, Vancouver,
887 British Columbia, Canada
- 888 Naveira Garabato, A. C., Frajka-Williams, E. E., Springy, C. P., Legg, S., Polzin, K. L., Forryan, A., et al.
889 (2019). Rapid mixing and exchange of deep-ocean waters in an abyssal boundary current. *Proceedings
890 of the National Academy of Sciences* 116, 13233–13238. doi:10.1073/pnas.1904087116
- 891 Nuttall, A. (1971). *Spectral estimation by means of overlapped fast fourier transform processing of
892 windowed data*. NUSC Tech. Rep. 4169, Naval Underwater Systems Center
- 893 Oakey, N. S. (1982). Determination of the rate of dissipation of turbulent kinetic energy from simultaneous
894 temperature and velocity shear microstructure measurements. *Journal of Physical Oceanography* 12,
895 256–271. doi:10.1175/1520-0485(1982)012
- 896 Osborn, T. R. (1974). Local vertical profiling of velocity microstructure. *Journal of Physical Oceanography*
897 4, 109–115. doi:10.1175/1520-0485(1974)004
- 898 Osborn, T. R. and Crawford, W. R. (1980). An airfoil probe for measuring turbulent velocity fluctuations
899 in water. In *Air-Sea Interaction: Instruments and Methods*, eds. F. W. Dobson and R. Davis (Plenum),
900 Mechanical Engineering. 535
- 901 Osborn, T. R., Farmer, D. M., Vagle, S., Thorpe, S. A., and Cure, M. (1992). Measurements of bubble
902 plumes and turbulence from a submarine. *Atmosphere-Ocean* 30, 419–440
- 903 Panchev, S. and Kesich, D. (1969). Energy spectrum of isotropic turbulence at large wavenumbers. *Comptes
904 rendus de l'académie Bulgare des sciences* 22, 627–630
- 905 Pope, S. B. (2009). *Turbulent Flows* (Cambridge University Press)
- 906 Roemmich, D., Alford, M. H., Claustre, H., Johnson, K., King, B., Moum, J., et al. (2019). On the future
907 of argo: A global, full-depth, multi-disciplinary array. *Frontiers in Marine Science* 6, 439
- 908 Roemmich, D., Boebel, O., Desaubies, Y., Freeland, H., King, B., LeTraon, P.-Y., et al. (1999). Argo: The
909 global array of profiling floats. *CLIVAR Exchanges* 13, 4–5
- 910 Roget, E., Lozovatsky, I., Sanchez-Martin, X., and Figueiroa, M. (2006). Microstructure measurements in
911 natural waters: Methodology and applications. *Progress in Oceanography - PROG OCEANOGR* 70,
912 126–148. doi:10.1016/j.pocean.2006.07.003
- 913 Siddon, T. E. (1965). *A turbulence probe utilizing aerodynamic lift*. Tech. Rep. 88, University of Toronto
- 914 Siddon, T. E. (1971). A miniature turbulence gauge for utilizing aerodynamic lift. *Review of Scientific
915 Instruments* 42, 653–656. doi:10.1063/1.1685193
- 916 Siddon, T. E. and Ribner, H. S. (1965). An aerofoil probe for measuring the transverse component of
917 turbulence. *J. American Inst. Aeronautics and Astronautics* 3, 747–749. doi:10.2514/3.2963
- 918 Sloyan, B. M., Wilkin, J., Hill, K. L., Chidichimo, M. P., Cronin, M. F., Johannessen, J. A., et al. (2019).
919 Evolving the physical global ocean observing system for research and application services through
920 international coordination. *Frontiers in Marine Science* 6, 449
- 921 Sreenivasan, K. R. (1995a). On the universality of the Kolmogorov constant. *Phys. Fluids* 7, 2778–2784.
922 doi:10.1063/1.868656
- 923 Sreenivasan, K. R. (1995b). On the universality of the Kolmogorov constant. *Physics of Fluids* 7,
924 2778–2784. doi:10.1063/1.868656

- 925 St. Laurent, L. S. M. (2017). Measurements of near-surface turbulence and mixing from autonomous ocean
926 gliders. *Oceanography* 30, 116–125. doi:10.5670/oceanog.2017.231
- 927 Taylor, G. (1935). Statistical theory of turbulence. *Proc. R. Soc. A* 151, 421–444. doi:10.1098/rspa.1935.
928 0158
- 929 Waterhouse, A. F., MacKinnon, J. A., Nash, J. D., Alford, M. H., Kunze, E., Polzin, H. L. S. K. L., et al.
930 (2014). Global patterns of diapycnal mixing from measurements of the turbulent dissipation rate. *Journal*
931 *of Physical Oceanography* 44, 1854–1872. doi:10.1175/JPO-D-13-0104.1
- 932 Wolk, F., Yamazaki, H., Seuront, L., and Lueck, R. G. (2002). A new free-fall profiler for measuring
933 bio-physical microstructure. *Journal of Atmospheric and Oceanic Technology* 19, 780–793. doi:10.
934 1175/1520-0426(2002)019
- 935 Wunsch, C. and Ferrari, R. (2004). Vertical mixing, energy, and the general circulation of the oceans.
936 *Annual Review of Fluid Mechanics* 36, 281–314. doi:{10.1146/annurev.fluid.36.050802.122121}

TABLES

Panel	P dbar	ε_1 -vsr W kg^{-1}	ε_1 -isr W kg^{-1}	ε_2 -vsr W kg^{-1}	ε_2 -isr W kg^{-1}	FOM_1	FOM_2
a	151.7	9.55×10^{-10}	3.77×10^{-10}	9.76×10^{-10}	8.62×10^{-10}	0.66	0.52
b	385.4	1.06×10^{-8}	7.82×10^{-9}	1.05×10^{-8}	7.36×10^{-9}	0.57	0.57
c	680	1.67×10^{-7}	1.46×10^{-7}	1.55×10^{-7}	1.34×10^{-7}	0.64	0.64
d	99.9	1.26×10^{-9}	4.73×10^{-9}	1.68×10^{-9}	4.70×10^{-9}	2.02	2.20

Table 1. Information about the selected spectra shown in Fig. 10. Dissipation estimates are given for both probes and using both methods of integration (vsr) and fit to inertial subrange (isr). FOM is for spectral integration.

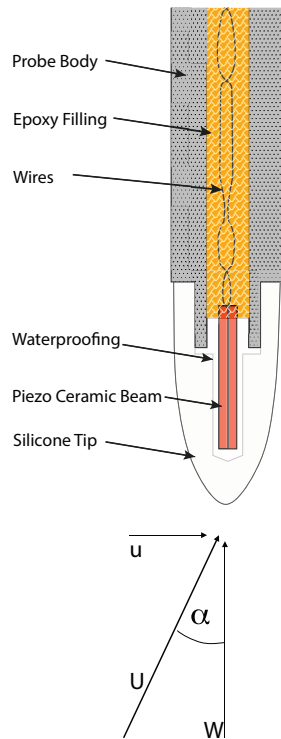
FIGURES

Figure 1. A sketch of the shear probe showing its main structural features and the expected incidental flow. The speed of profiling and the along-axis velocity is W , the cross-axis velocity is u , the angle of attack is α , and the total velocity is U . The force F of Eq.(1) is directed along u .

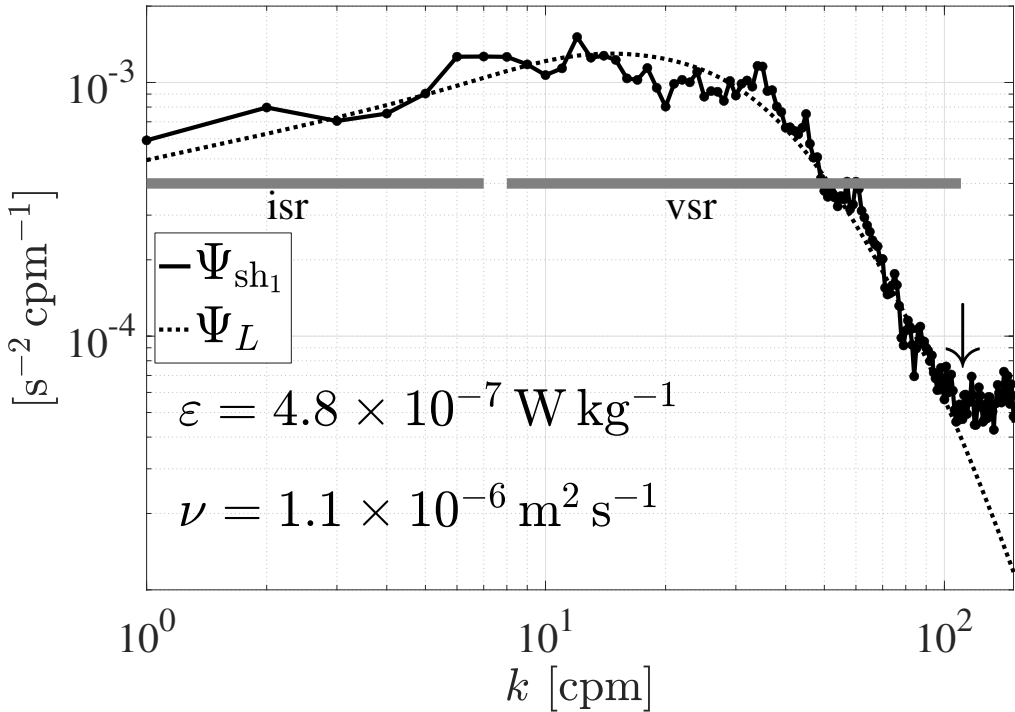


Figure 2. A typical spectrum of shear, Ψ_{sh_1} , that rises as $k^{1/3}$ in the inertial subrange (isr) and peaks and diminishes in the viscous subrange (vsr). This spectrum rises due to electronic noise at wavenumbers larger than 100 cpm (down arrow). Ψ_L is an analytic model of the spectrum after Lueck (2022a) for the indicated ε and ν .

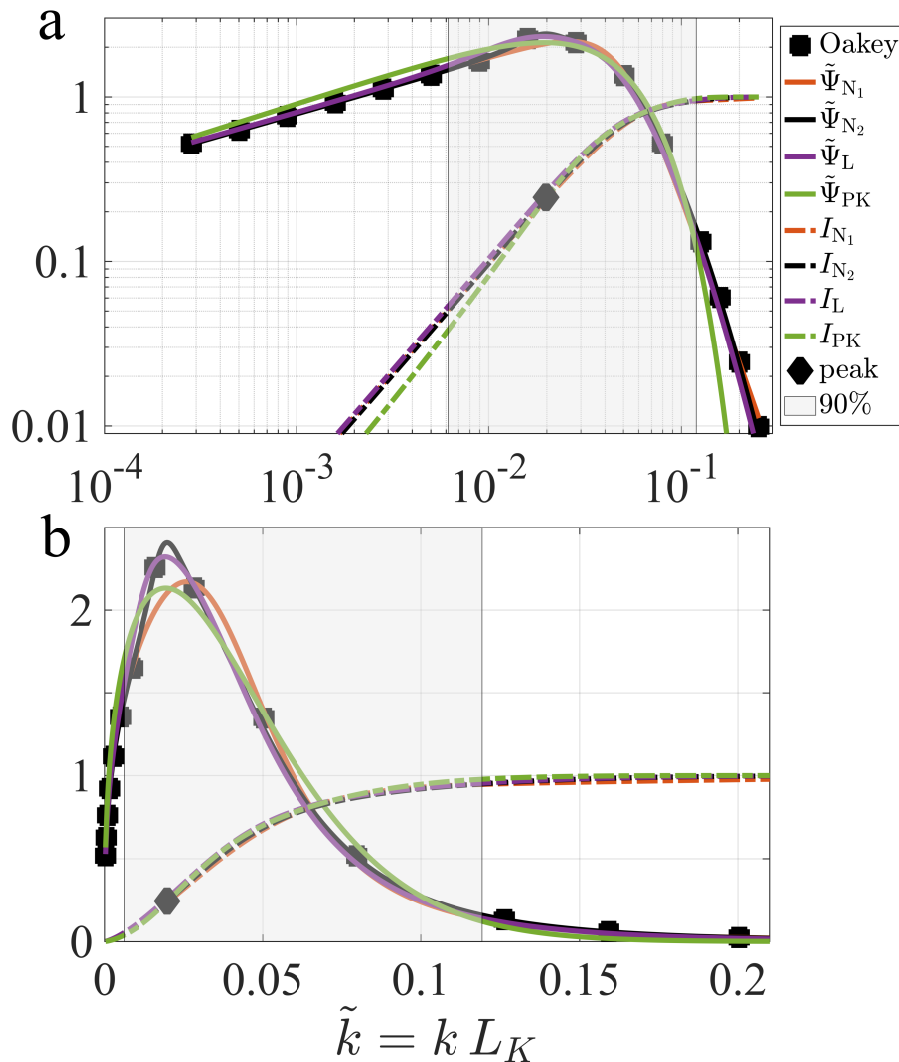


Figure 3. The non-dimensional shear spectral models and their approximations in logarithmic (a) and in linear form (b). The solid lines are the spectra $\tilde{\Psi}_{N_1}$ (red), $\tilde{\Psi}_{N_2}$ (black), $\tilde{\Psi}_L$ (maroon), $\tilde{\Psi}_{PK}$ (green). The dash-dot lines are the corresponding spectral integrals. The diamond marks the integral up to the peak of the spectra and equals ≈ 0.25 . The gray shading shows the range that contains 90 % of the shear variance.

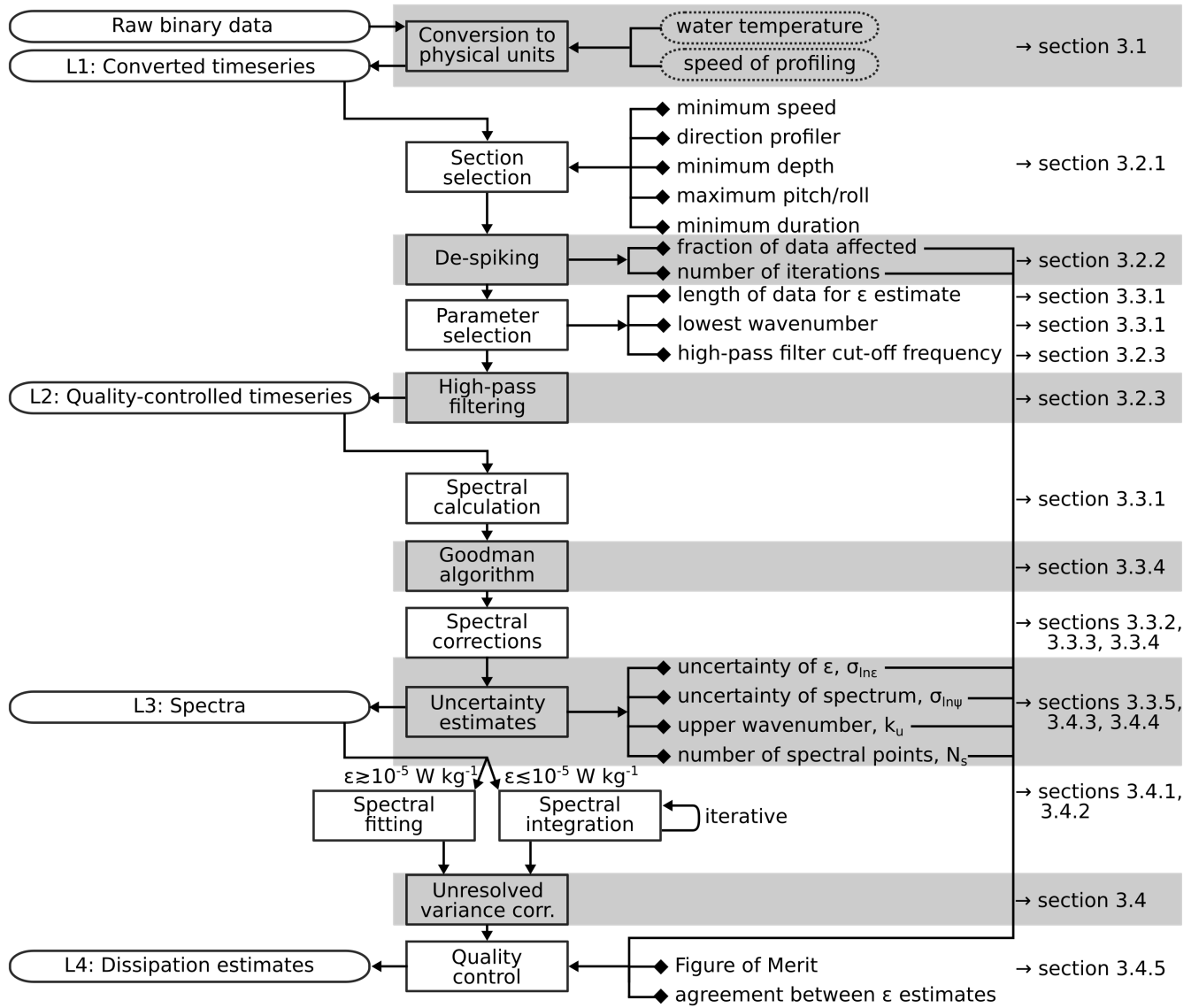


Figure 4. A schematic representation of the recommended processing of shear-probe data from levels L1 to L4. Details are provided in the sections shown on the right side.

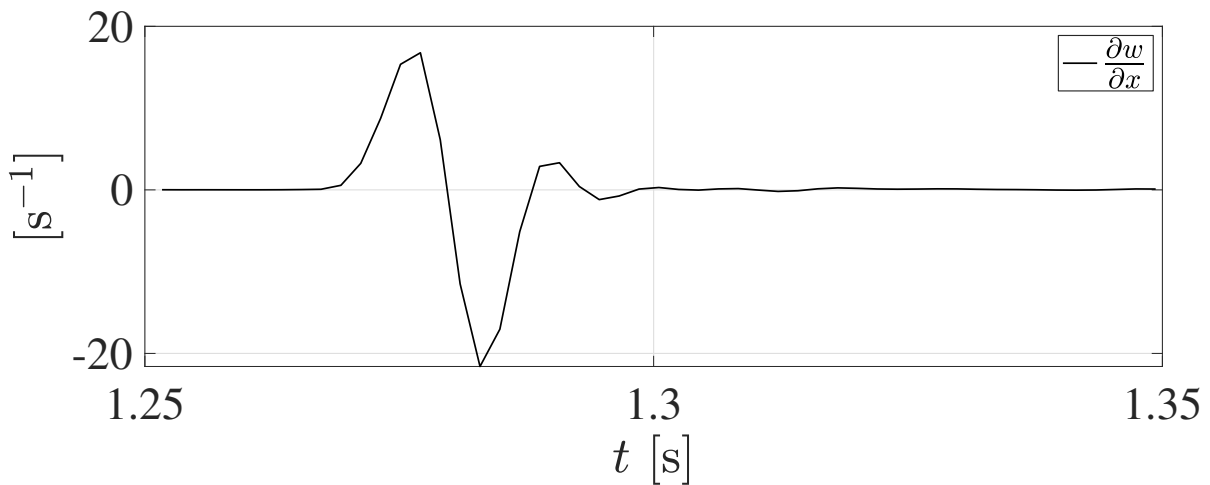


Figure 5. An example of a collision of the shear probe with zooplankton from a moored instrument.

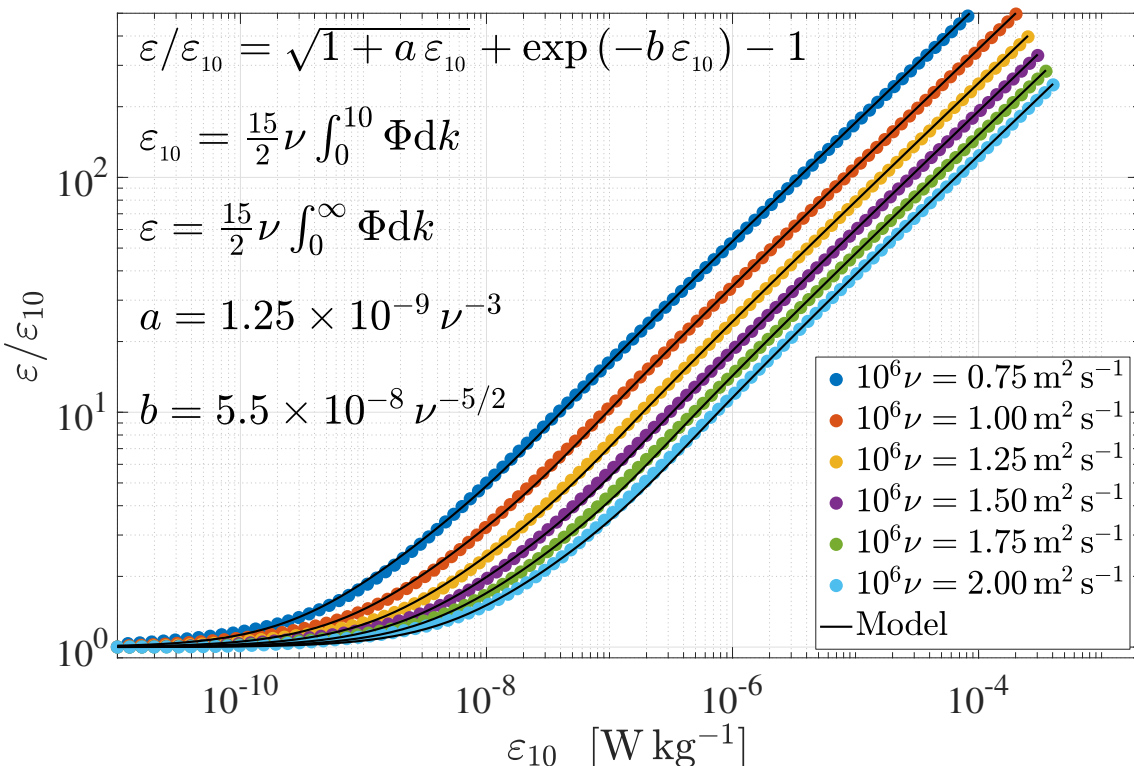


Figure 6. The rate of dissipation, ε , according to the Nasmyth model spectrum, relative to an estimate based on integrating this spectrum to 10 cpm, ε_{10} , as a function of ε_{10} for a range of viscosity, ν (colored disks) and an analytic approximation (black line).

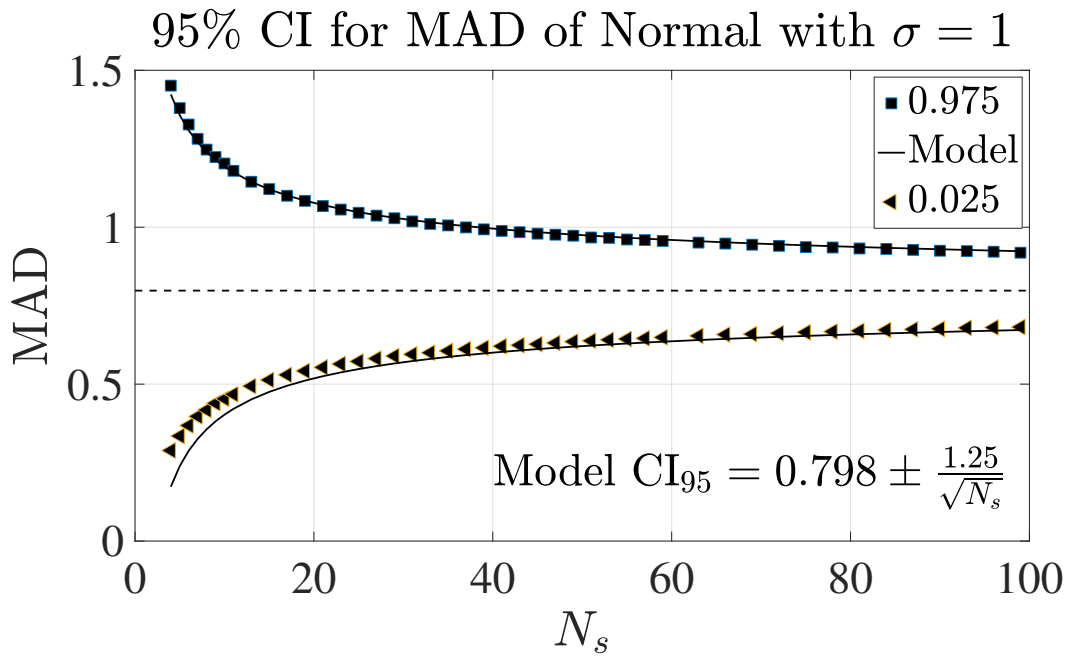


Figure 7. The 95 % confidence interval of the mean absolute deviation (MAD) of N_s samples drawn from a normal population with a standard deviation of $\sigma = 1$. The analytical model approximation is from (Lueck, 2022a)

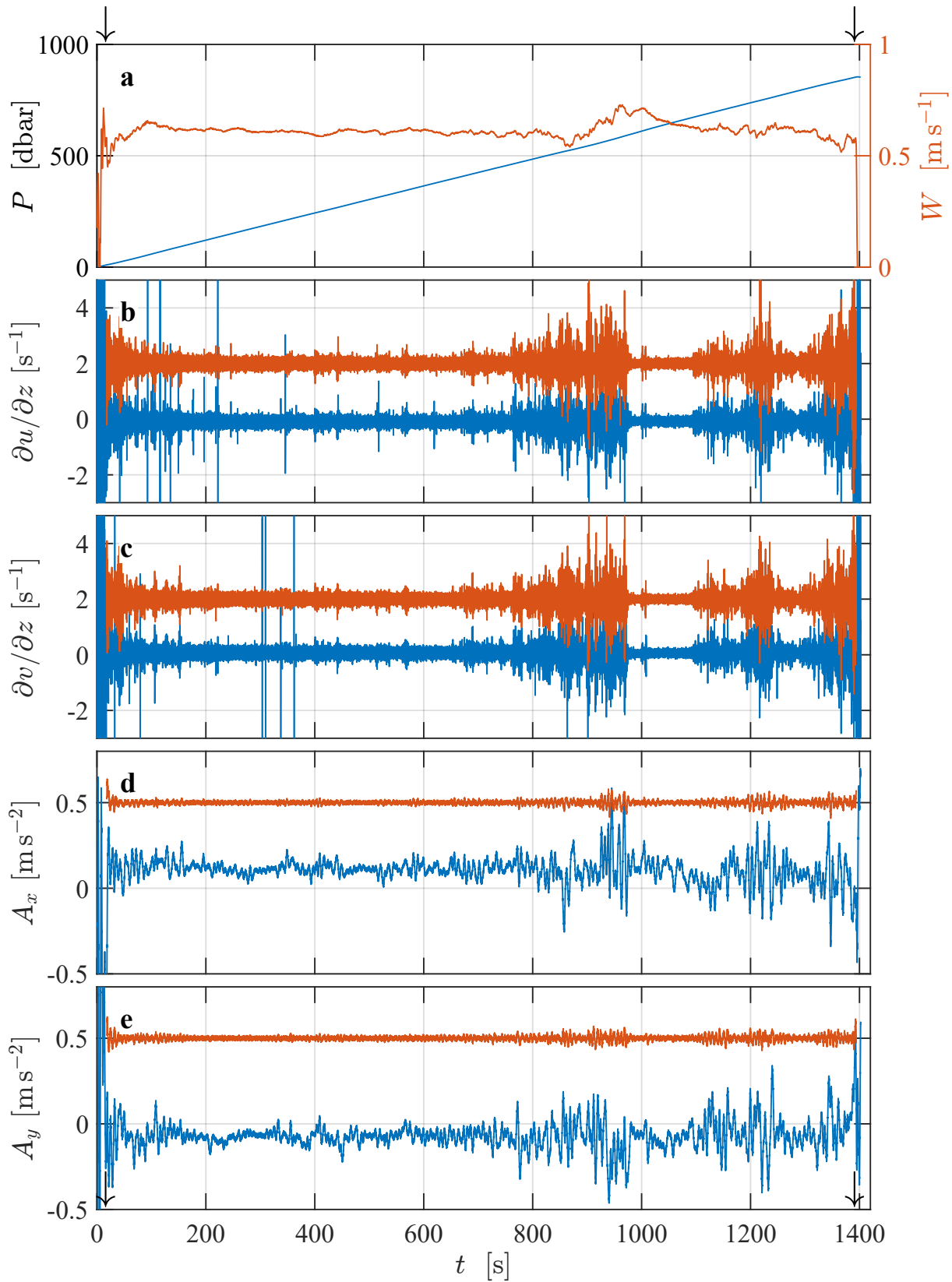


Figure 8. Time series of (a) pressure, P , and profiling speed, W ; high-pass filtered and de-spiked (b) $\partial u / \partial z$ and (c) $\partial v / \partial z$, and accelerations (d) A_x and (e) A_y (A_z not shown). De-spiked records are offset by 2 s^{-1} for shear and by 0.5 m s^{-2} for accelerations. Arrows in panels (a) and (e) mark the start and end of the selected section.

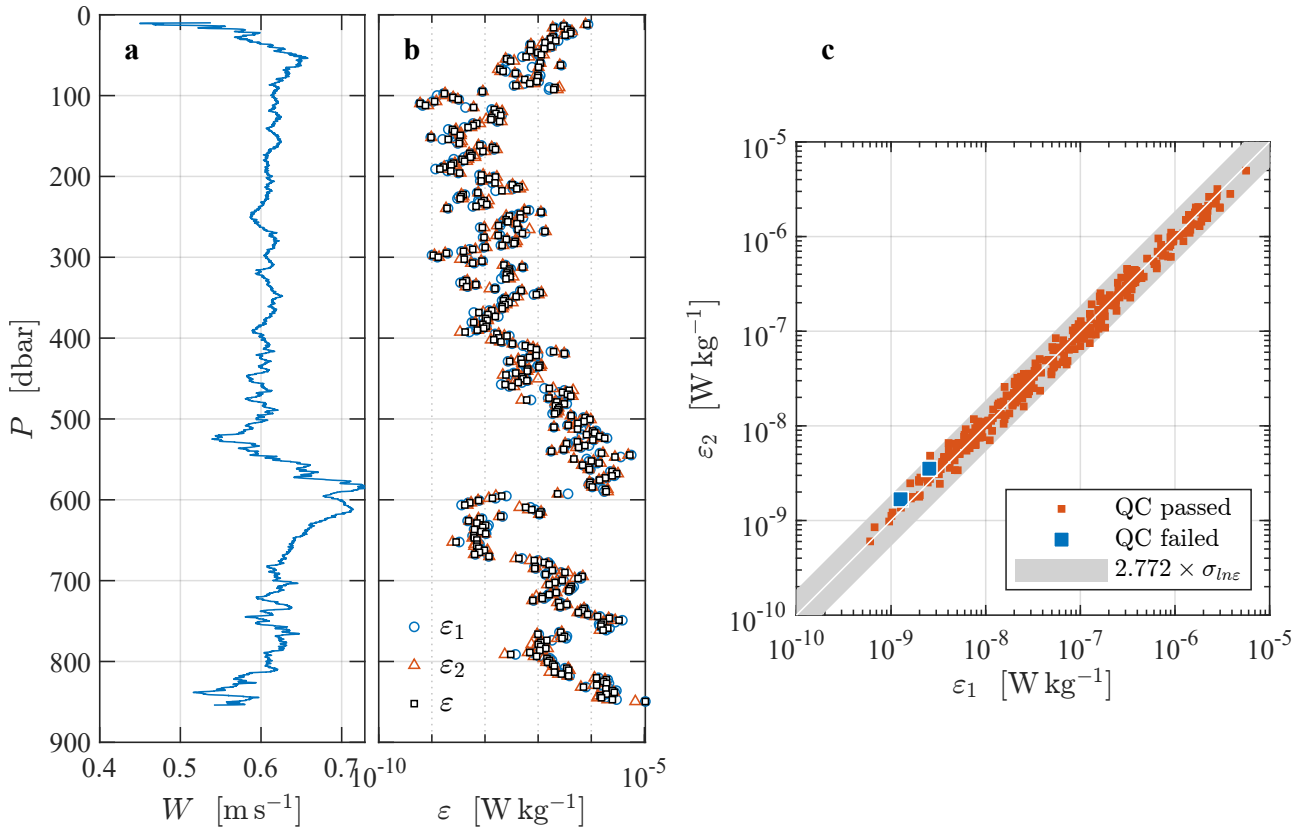


Figure 9. Dissipation estimates from the section of the time series shown in Fig. 8. (a) profiling speed, W , (b) dissipation estimates from probe 1 (blue circles) and 2 (red triangles), and the average of the estimates that passed QC (black squares). (c) Scatter plot of ε_1 against ε_2 for estimates that passed QC (red) and those that failed (blue). Gray band is the statistical uncertainty bounded by a factor of $2.772 \times \sigma_{\ln \varepsilon}$. The uncertainty of each ε estimate is determined by its actual $\sigma_{\ln \varepsilon}$ value, which ranges from 0.14 to 0.33 and averages to 0.23.

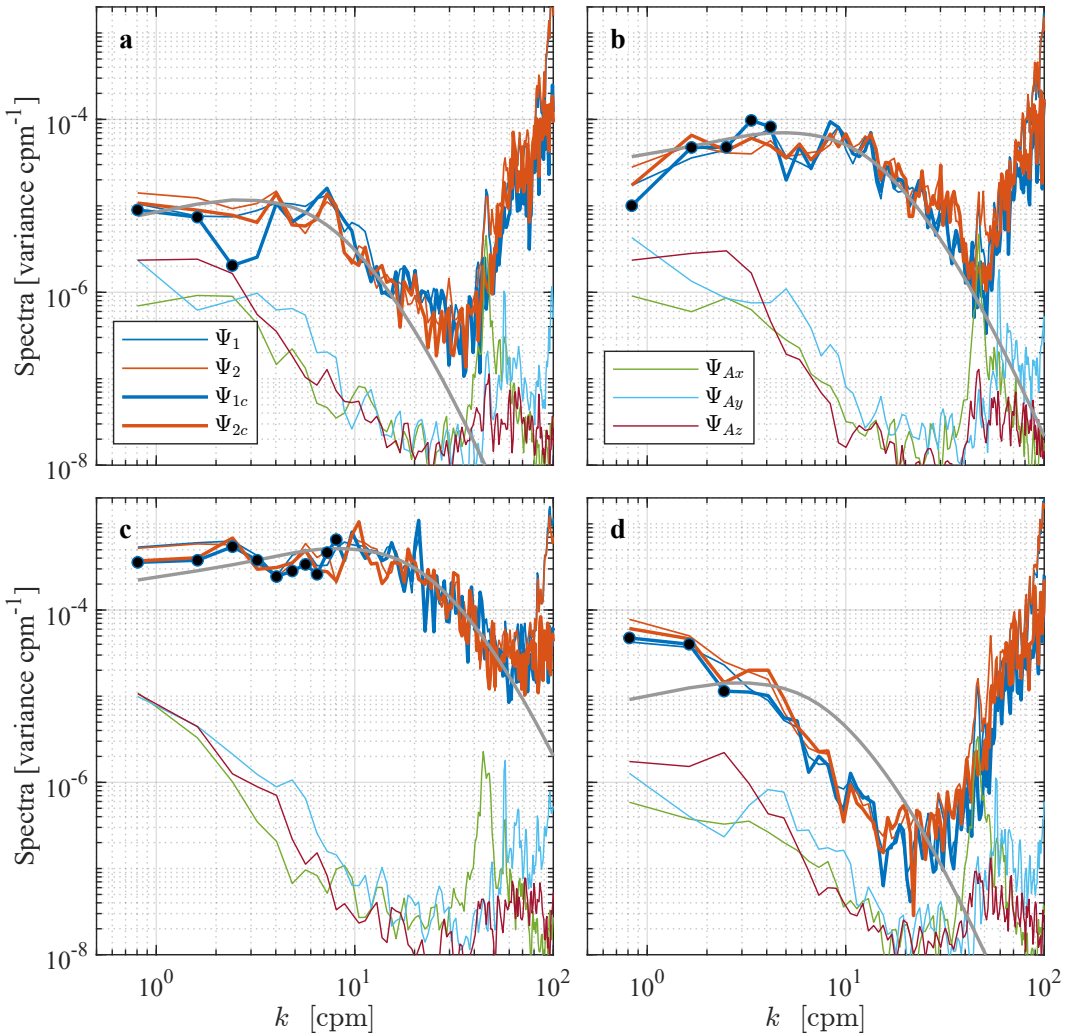


Figure 10. Wavenumber spectra from selected records (see Table 1). Wavenumbers are restricted to 100 cpm. Spectra are the measured (thin) and cleaned (thick) ones of shear probe 1 (blue) and 2 (red), acceleration (green, cyan, and magenta), and the spectrum of Lueck (2022a) (gray). Panels (a) to (c) are low, moderate and energetic turbulence, with both probes passing QC. The spectra in panel (d) fail the QC (FOM test) for both probes. Black dots are the spectral points within the inertial subrange used for alternative estimates using fitting to the inertial subrange.

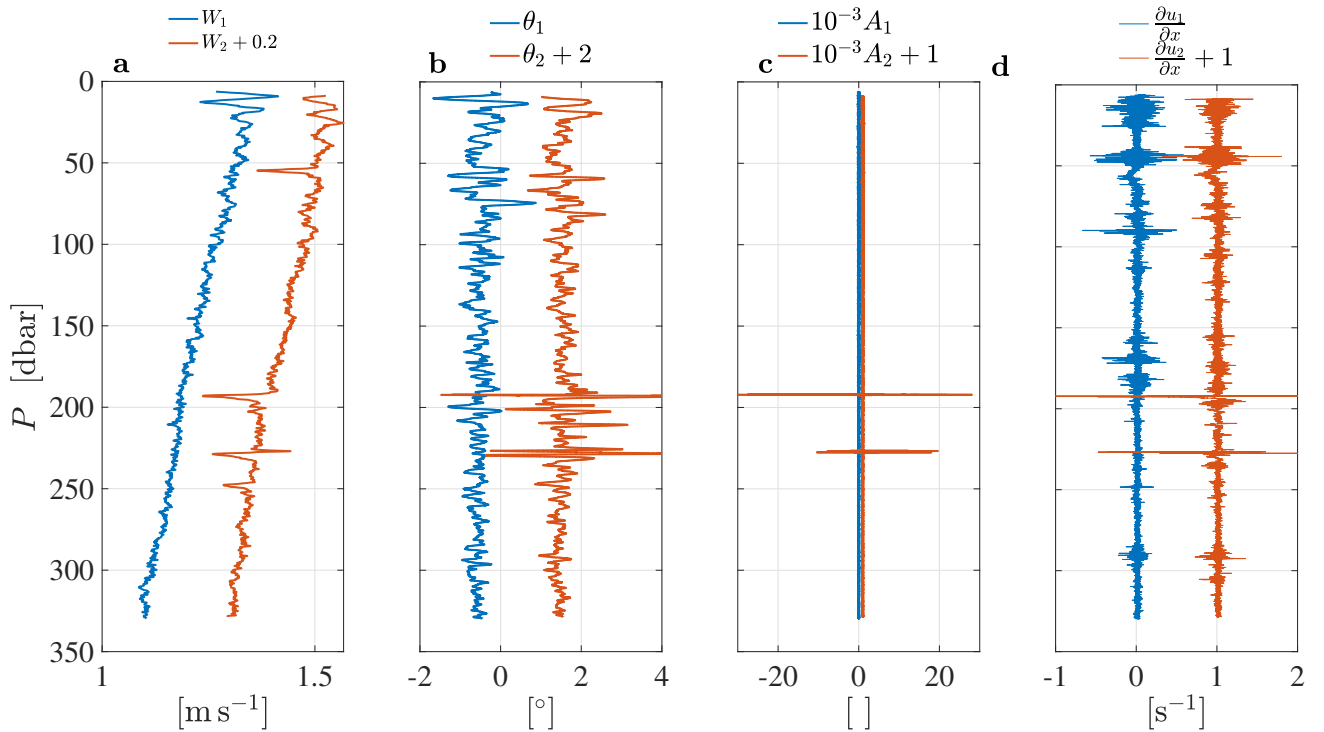


Figure 11. Two successive vertical profiles where the first (blue) was successful and the second (red) had a tether deployment problem. (a) The fall rate with four abrupt momentary decreases during the second profile. (b) The tilt of the profiler, (c) its vibrations and (d) the shear were all anomalously large near to 193 and 229 dbar.

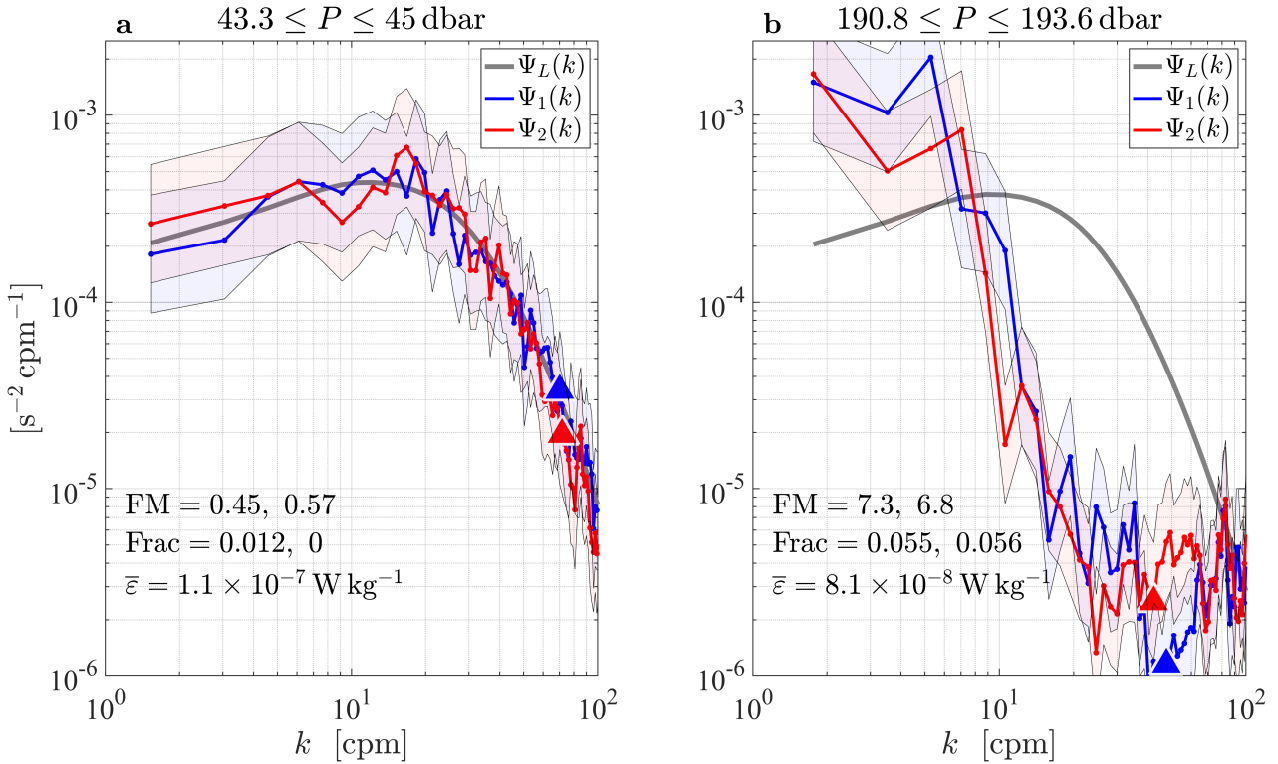


Figure 12. Spectra for the second profile shown in Fig. 11 for (a) the depth range without an anomalous fall-rate and (b) for the range of the anomaly near to 193 dbar. The spectra from probes 1 and 2 are blue and red, respectively, while the model spectrum after Lueck (2022a) is gray. The figure of merit (FOM), the fraction of data that was altered by the de-spiking routine (Frac), and the two-probe average rate of dissipation, $\bar{\varepsilon}$, are indicated within the figures. The wavenumber is restricted to 100 cpm. The triangles mark the upper wavenumber limit of spectral integration. The blue and red shading provide the 95 % confidence intervals for Ψ_1 and Ψ_2 , respectively.

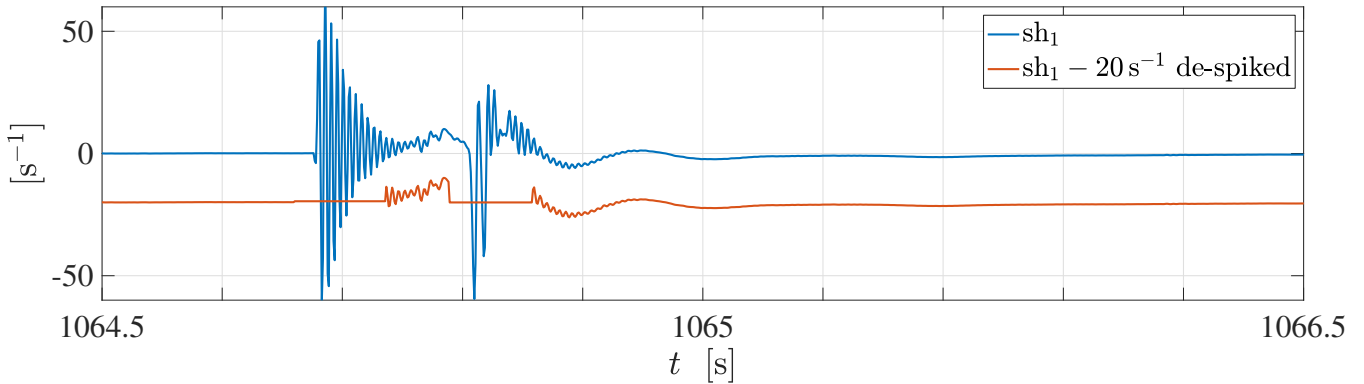


Figure 13. A close view of the original signal from shear probe 1 on the second section (profile) near to 193 dbar (blue) and this signal after it was de-spiked (red).